

# Multiple Hypothesis Testing Framework for Spatial Signals

Martin Gözl, *Student Member, IEEE*,

Abdelhak M. Zoubir, *Fellow, IEEE* and Visa Koivunen, *Fellow, IEEE*

## Abstract

The problem of identifying regions of spatially interesting, different or adversarial behavior is inherent to many practical applications involving distributed multisensor systems. In this work, we develop a general framework stemming from multiple hypothesis testing to identify such regions. A discrete spatial grid is assumed for the monitored environment. The spatial grid points associated with different hypotheses are identified while controlling the false discovery rate at a pre-specified level. Measurements are acquired using a large-scale sensor network. We propose a novel, data-driven method to estimate local false discovery rates based on the spectral method of moments. Our method is agnostic to specific spatial propagation models of the underlying physical phenomenon. It relies on a broadly applicable density model for local summary statistics. In between sensors, locations are assigned to regions associated with different hypotheses based on interpolated local false discovery rates. The benefits of our method are illustrated by applications to spatially propagating radio waves.

## Index Terms

Large-scale inference, multiple hypothesis testing, sensor networks, local false discovery rate, method of moments, density estimation, radial basis function interpolation

## I. INTRODUCTION

The literature on methods to estimate the exact value of a spatially varying phenomenon of interest across a certain area based on spatially sparse measurements is vast and comprehensive, see, e.g., [1]. While the numerical value of a specific quantity may itself be of interest, such as air temperature, precipitation or wind speed and direction when monitoring the weather, many problems require performing inferences and providing interpretations on the underlying phenomenon. Practical examples include applications in environmental monitoring (e.g. identifying regions with intolerably high emission levels), spectrum sensing (e.g. detecting regions where certain frequency bands are densely used or underutilized), smart buildings (e.g. determining areas with low oxygen levels), integrated sensing and communication (ISAC, one of the drivers of 6G wireless) or acoustics (e.g. describing the region with high ambient noise levels). This fundamental problem [2] is illustrated in Fig. 1.

The work of M. Gözl is supported by the German Research Foundation (DFG) under grant ZO 215/17-2.

M. Gözl and A. M. Zoubir are with the Signal Processing Group, TU Darmstadt, Germany. V. Koivunen is with the Department of Signal Processing and Acoustics, Aalto University, Espoo, Finland. E-mail: {goelz, zoubir}@spg.tu-darmstadt.de, visa.koivunen@aalto.fi.

Over the past two decades, the rapid development of ever cheaper and smaller sensors, as well as the rise of faster, lower latency and more reliable wireless connectivity standards have facilitated the deployment of large-scale sensor networks, a key technology in the Internet of Things (IoT). In this work, we propose a fully data-driven framework to directly infer spatial regions of *interesting*, *different* or *anomalous* behavior with quantitative statistical performance guarantees in terms of Type I errors using large-scale sensor networks. To this end, we model the spatial area of interest as a regular spatial grid. We formulate a multiple hypothesis testing (MHT) problem such that a decision on the state of the observed phenomenon is made at each grid point (also referred to as a *location*). We discriminate between the nominal state of the phenomenon, represented by the null hypothesis  $H_0$ , and any state that deviates from the nominal, represented by alternate hypotheses. While in many problems, one could distinguish various classes of anomalous, interesting or different behavior, we summarize everything that is not conform with the null hypothesis under the alternative  $H_1$ . *Sensors* (also referred to as *nodes*), capable of communicating with a cloud/fusion center (FC), are placed sparsely in distinct locations. No particular sensor distribution geometry or configuration is assumed.

The proposed method does not presume a specific parametric spatial signal propagation model. Neither does it require raw measurements to be exchanged among neighboring nodes, nor to be transmitted to the FC. Instead, each node communicates local information to the FC via a scalar quantity [3]. The communication of all raw measurements [1] is infeasible in the context of large-scale sensor networks due to constraints on bandwidth and energy consumption [3], [4]. While the former is particularly critical when a network is composed of many agents operating in a congested spectrum, the latter is a crucial requirement for a long sensor life span.

It may not be feasible to specify an accurate probability model for each node and its signal environment. The underlying probability models are learned from the data, which makes our method robust against modeling errors and suitable to a wide range of applications. However, incorporating specific models describing the underlying physics may be beneficial, as will be pointed towards the end of this paper.

We propose that each node condenses its measurements in a single local sufficient statistic, likelihood ratio or  $p$ -value. Large-scale sensor networks may be composed of heterogeneous types of devices. Hence, the statistic is chosen to allow for fusing the results among potentially very different sensors. The principal purpose of dedicated emission sensors, for example, is to record data and perform inference or learning. Contrarily, smartphones equipped with a good number of different sensors collect data as a by-product of normal operation. In addition, a suitable local summary statistic is simple to compute. This limits energy consumption and reduces the hardware requirements for individual nodes. Also, it refrains from strict assumptions on the local signal model. Useful summary statistics in the MHT framework include  $p$ -values,  $z$ -scores and (generalized) likelihood ratios. These sensor-level quantities are forwarded to the FC, which fuses the information to identify the local regions associated with different hypotheses. Our work differs from distributed inference [5], where a single binary decision on the state of the phenomenon across the entire area is made.

In dependence on the size of the monitored area and the desired spatial resolution, the number of grid points and hence decisions might easily reach the order of tens of thousands. To prevent a flood of false positives by testing for  $H_0$  a large number of times [6], we follow the principles of MHT, where choosing the alternative  $H_1$  is called

a *discovery* [7]. Performance guarantees are commonly provided w.r.t. the false discovery rate (FDR), which is the expected proportion of false discoveries among all discoveries, [8]. Controlling the FDR is similarly popular to constraining the false alarm probability in binary hypothesis testing. When the number of true positives increases, procedures that control the FDR allow more false positives than classic MHT methods applied, e.g., in [9]. Thus, controlling the FDR leads to a larger detection power.

Attempting to control the FDR in our spatial inference setup poses the following problem-specific challenges. First, local summary statistics are only available at the subset of grid points where the sensors are located, but decisions between  $H_0$  and  $H_1$  need to be made at every grid point. Second, the deployed method must scale well to large-scale sensor networks, i.e., its computational complexity remains moderate even for a large number of nodes. Finally, the method should allow for incorporating available side information into the decision process to increase the detection power.

The past work on FDR control in the context of spatial data has focused on testing a priori [10], [11] or a posteriori [12]–[15] formed groups of data. While these procedures typically rely on assumptions that may not be realistic [16], they do also not provide guarantees w.r.t. to the localization accuracy of the identified alternative area. Random field-based approaches like [17], [18] suffer from excessive computational cost if the number of nodes is large. We find the concept of the local false discovery rate (l<sub>fdr</sub>) [19]–[22] particularly suitable to deal with the aforementioned challenges. The l<sub>fdr</sub> is computed for each sensor and quantifies the risk of making a false discovery when accepting  $H_1$  at its location. Previous work [22]–[27] demonstrates its capability to incorporate available side information like spatial proximity into decision making.

The l<sub>fdr</sub>'s are computed from the local summary statistics. In addition, the l<sub>fdr</sub>'s rely on the joint probability density function (PDF) of the local summary statistics and the overall proportion of alternatives that are unknown in practice. These quantities need to be learned or estimated accurately from the data. This is often referred to as *l<sub>fdr</sub> estimation* in the MHT literature [22]. A variety of estimators exist, often assuming that the joint PDF belongs to the exponential family [22], [26], [28], [29]. Our novel contributions in this work are as follows.

- We formulate an l<sub>fdr</sub>-based framework as a flexible data-driven approach to accurately determine spatial regions of interest, difference or anomaly of a physical phenomenon.
- We propose a novel, highly computationally efficient method for computing l<sub>fdr</sub>'s. It bases upon an innovative mixture distribution model and the method of moments.
- We demonstrate that proper interpolation of the l<sub>fdr</sub>'s between sensors allows for inferring the state of the phenomenon even at locations between the sensors, where measurements are unavailable. Our proposed method scales well to spatial inference with large-scale sensor networks under strict statistical performance guarantees.

**Notation:** Throughout the paper, regular lowercase letters  $x$  denote scalars, whereas bold lowercase letters  $\mathbf{x}$ , bold uppercase letters  $\mathbf{X}$  and underlined bold uppercase letters  $\underline{\mathbf{X}}$  denote vectors, matrices and third order tensors, respectively.  $\mathbf{X}^{\frac{1}{2}}$  and  $\mathbf{X}^{\dagger}$  denote matrix square root and Moore-Penrose inverse. Calligraphic letters  $\mathcal{X}$  denote sets and  $[X] := 1, 2, \dots, X$  sets containing all positive integers  $\leq X$ .  $|\mathcal{X}|$  is the cardinality of set  $\mathcal{X}$  and  $\mathbb{1}\{\cdot\}$  denotes the indicator function. The Hadamard product operator is  $\odot$ , while  $\circ$  represents the outer product.  $f_X(x)$  denotes

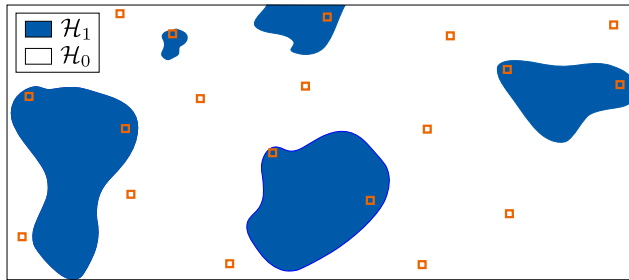


Figure 1: An exemplary spatial inference problem. Squares indicate sensors. The unknown region of interest  $\mathcal{H}_1$  consists of five spatially continuous subregions (blue). We discretize the entire observation area  $\mathcal{H}_0 \cup \mathcal{H}_1$  by a regular grid of  $Q$  points. The unknown binary local hypotheses  $H_q \in \{H_0, H_1\}$  represent the state of the phenomenon at each grid point  $q \in [Q]$ .  $\mathcal{H}_1$  is the set of all grid points where  $H_q = H_1$  holds.

the PDF of random variable (RV)  $X$  and  $f_{X|A}(x)$  its PDF conditioned on event A. FDR stands for the false discovery rate, lfd<sub>r</sub> for the local false discovery rate.

## II. THE SPATIAL INFERENCE PROBLEM

The spatial inference problem is illustrated in Fig. 1.  $\mathcal{H}_0$  and  $\mathcal{H}_1$  denote the regions of nominal and anomalous, different or interesting behavior, respectively. The continuous observation area is discretized by a regular grid of  $Q$  elements, to each of which we refer by its index  $q \in [Q]$ . Their position on the grid is denoted by  $\mathbf{c}_q = [c_{1,q}, c_{2,q}]^\top$ . The state of the observed phenomenon at grid point  $q \in [Q]$  and time instant  $t \in [T]$  is described by the unknown true binary local hypothesis  $H_{q,t} \in \{H_0, H_1\}$ , with the *null hypothesis*  $H_0$  and the *alternative*  $H_1$ . If  $H_{q,t} = H_0$ , we say that the observed phenomenon is in its nominal state at  $q \in [Q]$ ,  $t \in [T]$ . If  $H_{q,t} = H_1$ , an interesting phenomenon or *anomaly* is present.  $H_1$  holds under any deviation from  $H_0$  and is thus in general *composite*. In environmental monitoring,  $H_0$  could represent clean air, whereas  $H_1$  could indicate contamination above a tolerable level. We consider phenomena that vary smoothly in space and slowly in time. Due to the latter, we assume that the true local hypotheses are constant over the observation period and write  $H_q = H_{q,t} \forall t \in [T]$ . For now, we assume that a sensor is placed at each grid point.

$\mathcal{H}_1$  and  $\mathcal{H}_0$  are mutually exclusive sets that comprise the grid points at which  $H_0$  or  $H_1$  hold. Formally, the objective of spatial inference is to identify the set  $\mathcal{H}_0 = \{q \in [Q] \mid H_q = H_0\}$  of all grid points where  $H_0$  is in place, and the set  $\mathcal{H}_1 = \{q \in [Q] \mid H_q = H_1\}$  containing all locations where  $H_1$  holds. The models for the measured field levels  $y_q(t)$ ,  $q \in [Q]$ ,  $t \in [T]$ , differ under  $H_0$  and  $H_1$ , i.e.,

$$\begin{aligned} H_q = H_0 : \quad & y_q(t) = n_q(t), \\ H_q = H_1 : \quad & y_q(t) = x_q + n_q(t), \end{aligned} \tag{1}$$

where  $x_q \neq 0$  is the non-zero level of the phenomenon at location  $q$  and  $n_q(t)$  the temporally i.i.d. measurement noise. This noise process is spatially independent but not necessarily identically distributed in different nodes.  $x_q$  varies with  $q \in [Q]$ , but takes on similar values at close-by locations due to the spatial smoothness assumption. This is well-justified by the underlying mechanisms of many physical phenomena. Radio waves, for example, are subject

to path-loss and shadow fading [30] that vary slowly. We cannot directly observe  $H_q$ ,  $q \in [Q]$ . Eq. (1) suggests to utilize the measurements  $y_q(t)$ ,  $\forall t \in [T]$ , to obtain the empirical models for the hypotheses  $\hat{H}_q = H_0$  or  $\hat{H}_q = H_1$  and form the estimated regions  $\hat{\mathcal{H}}_0$  and  $\hat{\mathcal{H}}_1$  associated with null hypothesis and alternative. The individual sensors condense their raw observations over observation period  $T$  into soft local decisions statistics  $\tau_q$ ,  $q \in [Q]$ . These are more informative than local binary decisions, used, e.g., in [31]. A procedure that controls the FDR [8], the expected ratio between the number of false discoveries and all discoveries

$$\text{FDR} = \mathbb{E} \left[ \frac{\sum_{q \in \mathcal{H}_0} \mathbb{1}\{\hat{H}_q = H_1\}}{\sum_{q=1}^Q \mathbb{1}\{\hat{H}_q = H_1\}} \right], \quad (2)$$

at a nominal level  $\alpha$  guarantees that on average, a proportion  $(1 - \alpha)$  of the locations in  $\hat{\mathcal{H}}_1$  are actual members of the true alternative region  $\mathcal{H}_1$ .

The type of deployed sensor and the distribution of the measurement noise may differ from sensor to sensor [32]. Thus, the  $\tau_q$  cannot be directly fused with each other. Instead, one defines local summary statistics  $S_q$  that are normalized such that they are i.i.d.  $\forall q \in \mathcal{H}_0$ , but not necessarily for  $q \in \mathcal{H}_1$ . The null and alternative regions for a given set of observations  $\mathcal{S}^Q = \{s_1, \dots, s_Q\}$  of the local summary statistics  $S_1, \dots, S_Q$  can be inferred by standard methods, such as the Benjamini-Hochberg procedure (BH) [8].  $\mathcal{F}$  denotes the domain of  $S_q$ . Common choices for  $S_q$  are  $p$ -values

$$S_q := \int_{-\infty}^{\infty} f_{\tau_q|H_0}(\tau) d\tau = P_q, \quad (3)$$

$\forall q \in [Q]$ , where  $f_{\tau_q|H_0}(q)$  is the PDF of  $\tau_q$  under  $H_q = H_0$ , or  $z$ -scores  $S_q := \Phi^{-1}(P_q) = Z_q$ , where  $\Phi(\cdot)$  is the standard normal cumulative distribution function (CDF) [22]. For  $p$ -values, the domain is  $\mathcal{F} = [0, 1]$  and for  $z$ -scores,  $\mathcal{F} = \mathbb{R}$ .  $f_{\tau_q|H_0}(\tau)$  has to be known to compute  $p$ -values or  $z$ -scores. If  $f_{\tau_q|H_0}(\tau)$  is unknown, it can be estimated from the data using for example the bootstrap [33], [34]. Small  $p$ -values indicate very little support for the null hypothesis.

We propose to solve the spatial inference problem with the help of a suitable MHT soft decision statistic. Define the random variable  $S$  that represents the mixture of all local summary statistics. The PDF of  $S$  is

$$f_S(s) = \pi_0 f_{S|H_0}(s) + (1 - \pi_0) \sum_{q \in \mathcal{H}_1} f_{S_q|H_1}(s), \quad (4)$$

with  $\pi_0 = |\mathcal{H}_0|/Q$  the relative size of the null region,  $f_{S|H_0}(s)$  the PDF for  $S_q \forall q \in \mathcal{H}_0$  and  $f_{S_q|H_1}(s)$  the PDF for  $S_q$  if  $q \in \mathcal{H}_1$ . The model in Eq. (4) exploits that the local summary statistics are i.i.d. across locations  $q \in \mathcal{H}_0$ . Finally, the local false discovery rate is [20], [22]

$$\text{lfdr}(s) = \frac{\pi_0 f_{S|H_0}(s)}{f_S(s)}. \quad (5)$$

Appealingly,  $\text{lfdr}_q = \text{lfdr}(s_q)$  is the posterior empirical Bayes probability that  $q \in \mathcal{H}_0$ . Thus, it allows us to assess the probability of making a false discovery. To solve the spatial inference problem while controlling  $\text{FDR} \leq \alpha$ , we form the region associated with the alternative hypothesis

$$\hat{\mathcal{H}}_1 = \operatorname{argmax}_{\mathcal{H} \subseteq [Q]} \left\{ |\mathcal{H}| : \sum_{q \in \mathcal{H}} \text{lfdr}_q \leq \alpha \right\}. \quad (6)$$

This approach guarantees FDR control at level  $\alpha$  while maximizing detection power, since the so-called Bayesian

false discovery rate (BFDR)  $\text{BFDR}(\hat{\mathcal{H}}_1) = \sum_{q \in \hat{\mathcal{H}}_1} \text{lfdr}_q$  is an upper bound of the Frequentist FDR from Eq. (2) [22]. Note that the BFDR is the average false discovery probability *across the alternative region*  $\hat{\mathcal{H}}_1$ , while the *lfdr* asserts each location  $q \in [Q]$  with the *individual* risk of being a false discovery.

In what follows, we develop a novel method to compute the *lfdr*'s. The concept of the local false discovery rate is described in Sec. III. The proposed method is based on a sophisticated probability model for the local summary statistics. We introduce the novel model and a novel algorithm to compute *lfdr*'s from observed data in Sec. IV. To determine decision statistics in between the sparse sensor locations, we propose to interpolate the sensor *lfdr*'s in Sec. V. We conclude by simulation results in Sec. VI.

### III. LOCAL FALSE DISCOVERY RATE ESTIMATION

Inference based on local false discovery rates contains estimation and hypothesis testing components, since the theoretical *lfdr*'s defined in Eq. (5) are unavailable in practice. Thus, the null and alternative regions are determined based on *lfdr* estimates. The accuracy of the deployed estimators has immediate consequences on FDR control: underestimation of the *lfdr*'s leads to violations of the nominal FDR level, whereas overestimation reduces power.

The general structure of *lfdr* estimators follows from Eq. (5). The PDF of  $S$  for  $q \in \mathcal{H}_0$  is most often assumed to be known [22]. The relative size of the null region  $\pi_0$  is unknown. Finally, the mixture distribution  $f_S(s)$  from Eq. (4) is not available. The common approach to *lfdr* estimation relies on separate estimation of  $\pi_0$  and  $f_S(s)$  by estimators  $\hat{\pi}_0$  and  $\hat{f}_S(s)$ , which are then plugged into Eq. (5) [22], i.e.,

$$\hat{\text{lfdr}}(s) = \frac{\hat{\pi}_0 f_{S|\mathcal{H}_0}(s)}{\hat{f}_S(s)}. \quad (7)$$

The underlying physical effects drive the statistical behavior of the *lfdr* via  $f_S(s)$ . Thus, a generally optimal estimator  $\hat{\text{lfdr}}(s)$  does not exist.

The increasing interest in the incorporation of covariate information into MHT, e.g. [23]–[26], [35], has lead to a number of sophisticated *lfdr* estimators that treat  $f_S(s)$  as a two component mixture, the so-called two groups model [19], [36]

$$\hat{f}_S(s) = \hat{\pi}_0 f_{S|\mathcal{H}_0}(s) + (1 - \hat{\pi}_0) \hat{f}_{S|\mathcal{H}_1}(s). \quad (8)$$

We also adopt the two-groups model. In spatial inference,  $\hat{f}_{S|\mathcal{H}_1}(s)$  is an estimator for the mixture of local summary statistics in the alternative region  $f_{S|\mathcal{H}_1}(s) = \sum_{q \in \mathcal{H}_1} f_{S_q|\mathcal{H}_1}(s)$ , see Eq. (4).

#### A. The choice of a local summary statistic

We infer the alternative region  $\hat{\mathcal{H}}_1$  for a given set of realizations of the local summary statistics  $\mathcal{S}^Q = \{s_1, \dots, s_Q\}$  by Eq. (6) with  $\text{lfdr}_1, \dots, \text{lfdr}_Q$ . We follow the traditional approach to *lfdr* estimation.  $\text{lfdr}(s) = \text{lfdr}_q$  is found from Eq. (7) using plug-in estimates  $\hat{\pi}_0$  and  $\hat{f}_S(s)$ . The latter obeys the two groups model from Eq. (8).  $f_{S|\mathcal{H}_0}(s)$  is assumed to be known, while the behavior in the alternative region is captured by  $\hat{f}_{S|\mathcal{H}_1}(s)$ . If the *lfdr*'s are underestimated at locations in  $\hat{\mathcal{H}}_1$ , the nominal FDR level  $\alpha$  is violated. Thus, on average more than a fraction  $\alpha$  of the members in  $\hat{\mathcal{H}}_1$  are false positives.

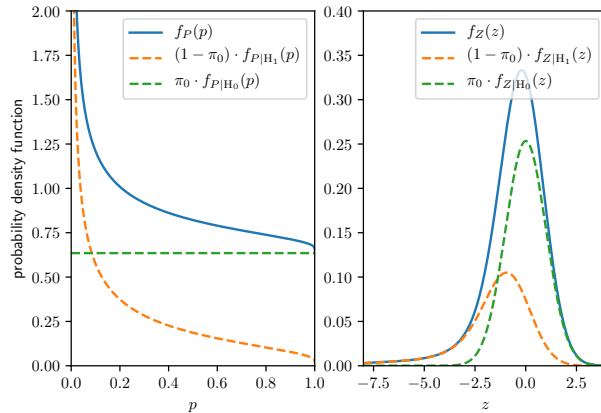


Figure 2: The true PDFs  $f_P(p)$  and  $f_Z(z)$  for  $p$ -values and  $z$ -scores from Sc. B described in Sec. VI. The two-groups model from Eq. (8) always holds, i.e.,  $f_S(s)$  is composed of a null and an alternative component.  $f_{P|H_0}(p)$  and  $f_{Z|H_0}(z)$  are known analytically. The mixture proportion  $\pi_0$  and the true  $f_{P|H_1}(p)$  and  $f_{Z|H_1}(z)$  are unknown. In general, the alternative component for one-sided  $p$ -values is a monotonically decreasing function. For one-sided  $z$ -scores, the alternative component exhibits a heavy left tail.

The suitability of different density estimation techniques to determine  $\hat{f}_S(s)$  depends on the local summary statistic. The two groups model from Eq. (8) applies to  $p$ -values and  $z$ -scores alike. As illustrated in Fig. 2, the shapes of  $f_S(s)$ ,  $f_{S|H_0}(s)$  and  $f_{S|H_1}(s)$  differ significantly. For  $p$ -values,  $f_{S|H_0}(s) = f_{P|H_0}(p)$  follows an  $\mathcal{U}[0, 1]$ . For  $z$ -scores,  $f_{S|H_0}(s) = f_{Z|H_0}(z)$  is the standard normal distribution,  $\phi(z)$ .

Much of the existing literature on lfr estimation focuses on  $z$ -scores.  $\hat{f}_Z(z)$  is often modeled as a parametric PDF with infinite support  $Z \in \mathcal{F} = \mathbb{R}$ .  $\hat{f}_Z(z)$  is found by estimating the parameters of a finite Gaussian mixture model [37] or an exponential family model [22], [28]. The decomposition of  $\hat{f}_Z(z)$  into  $\hat{\pi}_0 f_{Z|H_0}(z)$  and  $(1 - \hat{\pi}_0) \hat{f}_{Z|H_1}(z)$  for Eq. (8) is to be performed in a subsequent, non-trivial step. Non-parametric methods, which directly decompose  $\hat{f}_Z(z)$  into the components of the two-groups model have been studied using kernel estimates [38] and, more recently, predictive recursion [26], [29], [39], [40].

To maintain FDR control, the estimator of  $\hat{f}_Z(z)$  is required to be highly accurate for values of  $z \in \mathcal{F}$  that are more likely under the alternative, that is, in the left tail for left-sided  $z$ -scores. High tail accuracy of the estimate  $\hat{f}_Z(z)$  is difficult to achieve, especially at small sample sizes. An overall well-fitting  $\hat{f}_Z(z)$  does not necessarily imply a good fit in the tails, due to their small probability mass. Tail behavior is difficult to capture. Finally, the domain of  $z$ ,  $\mathcal{F} = \mathbb{R}$ , covers the entire real axis. Hence, the support of  $f_Z(z)$  and its tails is infinite.

The lfr estimators based on  $p$ -values are not subject to the previously discussed tail-accuracy-related issues of  $z$ -score-based lfr estimators. To this end, observe that the assumption of uniformly distributed  $p$ -values under  $H_0$ , i.e.,  $f_{P|H_0}(p)$  follows  $\mathcal{U}[0, 1]$ , spreads statistically insignificant observations uniformly across the bounded domain  $\mathcal{F} = [0, 1]$  instead of producing a bulk in the center of the domain. Consequently, most of the mass of  $f_P(p)$  is located in the subregion of  $\mathcal{F}$  that contains statistically significant (small)  $p$ -values, i.e., where  $f_{P|H_1}(p)$  is large. Additionally,  $p$ -value-based lfr estimation allows for a simple way [36] to decompose estimate  $\hat{f}_P(p)$  into the

components of the two-groups model  $\hat{\pi}_0 f_{P|H_0}(p) = \hat{\pi}_0$  and  $\hat{f}_{P|H_1}(p)$ ,  $p \in \mathcal{F} = [0, 1]$ ,

$$\hat{\pi}_0 = \min \hat{f}_P(p), \quad \hat{f}_{P|H_1}(p) = \frac{\hat{f}_P(p) - \hat{\pi}_0}{1 - \hat{\pi}_0}. \quad (9)$$

Since the domain of the  $p$ -values  $\mathcal{F} = [0, 1]$  is bounded,  $p$ -value density estimators are commonly parametric. The true analytical form of  $f_P(p)$  is unknown. Consequently, one has to identify a parametric probability model  $f_P^\theta(p)$  and a parameter vector value  $\hat{\theta}$  such that  $f_P^{\hat{\theta}}(p) \approx f_P(p)$ . The quality of the PDF estimate  $\hat{f}_P(p) = f_P^{\hat{\theta}}(p)$  can be evaluated by difference measures  $d(f_P(p), \hat{f}_P(p))$ , such as the Kullback-Leibler (KL) divergence or the Wasserstein (WS) distance.

Since our proposed method relies on modeling  $p$ -value mixture distributions, we consider the popular beta-and-uniform mixture (BUM) model [36],

$$f_P^{\text{BUM}}(p) = w + (1 - w) \text{beta}(a) = w + (1 - w)ap^{a-1}. \quad (10)$$

Superscript BUM indicates the dependency on the BUM parameters  $w \in [0, 1]$  and  $a \in (0, 1)$ .  $\hat{f}_P^{\text{BUM}}(p)$  denotes the BUM model with the respective maximum likelihood estimator (MLE)  $\hat{w}$  for  $w$  and  $\hat{a}$  for  $a$ . The BUM model exploits two known properties of  $f_P(p)$ , which are also apparent in Fig. 2. First, the uniform distribution under  $H_0$  is captured by the constant  $w$ . Second,  $f_{P|H_1}(p)$  is known to be monotonically decreasing. A single-parameter beta distribution decreases monotonically  $\forall a \in (0, 1)$ . The BUM model is simple and has been applied successfully in a number of applications. However, it lacks flexibility due to its limited number of tuning parameters. Estimating  $f_P(p)$  by  $\hat{f}_P(p) = \hat{f}_P^{\text{BUM}}(p)$  leads to overly pessimistic lfd<sub>r</sub> estimates, as the simulations in Sec. VI underline. We introduce a more flexible model in Sec. IV.

#### IV. THE PROPOSED LFDR ESTIMATOR

In this section, we introduce a novel lfd<sub>r</sub> estimator. Our approach estimates lfd<sub>r</sub>'s from  $p$ -values. We propose the parametric probability model

$$f_P^{\text{BM}}(p) = \sum_{l=1}^L w^{(l)} \text{beta}(a^{(l)}), \quad (11)$$

a finite single-parameter beta distribution mixture (BM) with shape parameters  $a^{(l)} \in \mathbb{R}_{>0}$  and mixture weights  $w^{(l)} \in [0, 1]$ ,  $\forall l \in [L]$  such that  $\sum_{l=1}^L w^{(l)} = 1$  and  $L < \infty$ . For  $a^{(l)} < 1$ ,  $a^{(l)} = 1$  and  $a^{(l)} > 1$ , the  $l$ -th component  $\text{beta}(a^{(l)})$  is monotonically decreasing, constant and monotonically increasing in  $p \in [0, 1]$ , respectively. Due to the increased number of components,  $f_P^{\text{BM}}(p)$  is more flexible than  $f_P^{\text{BUM}}(p)$ . Estimating its parameters is more involved than for the BUM model, since  $2L - 1$  model parameters are to be determined from the observations  $\mathcal{P}^Q = \{p_1, \dots, p_Q\}$ . Closed-form MLEs for the parameters of mixture distributions are difficult to obtain. Instead, MLEs are commonly found iteratively by expectation-maximization (EM) [41], which is computationally expensive for larger model orders. Also, the parameter estimates are only locally optimal, which may result in poorly fitting models for non-convex likelihood functions. In this work, we target computationally light-weighted procedures suitable for large-scale sensor networks. Our approach bases upon the method of moments (MoM) that estimates model parameters by solving pre-defined equation systems.



### A. The method of moments

The principle of moment-based parameter estimation [42], [43] is to match population and empirical moments. To this end, multivariate systems of moment equations are solved. The MoM is conceptionally simple, but also entails challenges. Its analytic complexity rapidly increases with the number of model parameters. In addition, empirical higher-order moments are prone to large variance [44]. Therefore, the sample size required to provide meaningful estimates grows exponentially in the number of model parameters [45]. As a consequence, the standard MoM is not well-suited to determining the parameters for Eq. (11).

The spectral method of moments (sMoM), a recent approach [45], [46], allows to determine the parameters of multivariate Gaussian mixtures from only the first three moments. Thus, sMoM avoids higher-order moments. In contrast to other work on the field of low-order moment-based parameter estimation, the method in [45] does not require a minimum distance between the locations of the mixture components to guarantee identifiability. This suits particularly well to this work, since we are dealing with  $p$ -values on the domain  $\mathcal{F} = [0, 1]$  and need to discriminate between mixture components that are located closely to one another. Combining the BM model and the sMoM provides a base for a computationally efficient  $p$ -value density estimator that we introduce in what follows.

### B. The multivariate $p$ -value model

Traditional statistical techniques would treat the input data  $\mathcal{P}^Q = \{p_1, \dots, p_Q\}$  as a single observation of a  $Q$ -dimensional random vector with elements  $P_q, q \in [Q]$ . The identification of the regions associated with null hypothesis and alternative  $\mathcal{H}_0$  and  $\mathcal{H}_1$  based on a single observation of a high-dimensional random vector is fairly challenging. To perform spatial inference, we adopt the idea of *learning from the experience of others* [22] and treat  $\mathcal{P}^Q$  as  $Q$  realizations of the same scalar random variable  $P \sim f_P(p)$ . We first model the  $p$ -values as a  $d$ -dimensional random vector  $\mathbf{p}$  instead of estimating  $f_P(p)$  directly from  $\mathcal{P}^Q$ . Then, we estimate its joint PDF  $f_{\mathbf{p}}(\mathbf{p})$ . Finally, we average over the  $d$  marginals to obtain the univariate estimate  $\hat{f}_P(p)$ . Estimating a joint PDF appears intuitively more challenging. However, our multivariate  $p$ -value model enables fast and reliable estimation of  $f_P(p)$ , since it facilitates the application of the sMoM. To the best of our knowledge, this concept is entirely new to lfdR estimation.

In what follows, assume  $P \sim f_P(p) = f_P^{\text{BM}}(p)$ . We divide the set of observations  $\mathcal{P}^Q = \{p_1, \dots, p_Q\}$  for random variable  $P \sim f_P^{\text{BM}}(p)$  into  $M$  distinct subsets  $\mathcal{P}_1^d, \dots, \mathcal{P}_M^d$  of equal size  $d$ ,  $M = \lfloor Q/d \rfloor$ . Next, arrange the elements of each  $\mathcal{P}_m^d$  in no particular order into  $M$   $d$ -dimensional  $p$ -value vectors  $\mathbf{p}_m \forall m \in [M]$ .  $\mathbf{p}_1, \dots, \mathbf{p}_M$  are observations of the random vector  $\mathbf{p} \sim f_{\mathbf{p}}(\mathbf{p})$ , whose  $i$ -th entry be random variable  $\tilde{P}_i, i \in [d]$ . Since  $P \sim f_P^{\text{BM}}(p)$ , the marginal distribution of each  $\tilde{P}_i$  can be described without loss of generality by a  $K$ -component mixture

$$\tilde{P}_i \sim \sum_{k=1}^K w^{(k)} \text{beta}(a_i^{(k)}), \quad (12)$$

with mixture proportion vector  $\mathbf{w} = [w^{(1)}, \dots, w^{(K)}]^\top$  such that  $\sum_{k=1}^K w^{(k)} = 1$  and shape parameters  $a_i^{(k)} \in \mathbb{R}_{>0}$ . The partitioning of  $\mathcal{P}^Q$  into  $\mathcal{P}_1^d, \dots, \mathcal{P}_M^d$  and the ordering of the entries within each  $\mathbf{p}_m, m \in [M]$ , is not to be based  $p_q, q \in [Q]$ . Then, the  $\tilde{P}_i \forall i \in [d]$  are mutually independent random variables. Thus,  $f_{\mathbf{p}}(\mathbf{p})$  is fully characterized

by its marginals, which relate to  $f_P^{\text{BM}}(p)$  through

$$f_P^{\text{BM}}(p) = d^{-1} \sum_{k=1}^K w^{(k)} \sum_{i=1}^d \text{beta}(a_i^{(k)}). \quad (13)$$

With [47, Chapter 24], the first two cumulants, mean  $\kappa_{1_i}^{(k)}$  and variance  $\kappa_{2_i}^{(k)}$ , of the  $i$ -th marginal's  $k$ -th component are found  $\forall i \in [d], \forall k \in [K]$ , as

$$\kappa_{1_i}^{(k)} = \frac{a_i^{(k)}}{a_i^{(k)} + 1}, \quad \kappa_{2_i}^{(k)} = \frac{a_i^{(k)}}{a_i^{(k)} + 2} - \left( \frac{a_i^{(k)}}{a_i^{(k)} + 1} \right)^2. \quad (14)$$

The third-order cumulant, is

$$\kappa_{3_i}^{(k)} = \frac{a_i^{(k)}}{a_i^{(k)} + 3} - \frac{3a_i^{(k)}}{(a_i^{(k)} + 2)} \frac{a_i^{(k)}}{(a_i^{(k)} + 1)} + 2 \left( \frac{a_i^{(k)}}{a_i^{(k)} + 1} \right)^3. \quad (15)$$

Additionally, denote the  $k$ -th mixture component mean vector by  $\boldsymbol{\kappa}_1^{(k)} = [\kappa_{1_1}^{(k)}, \dots, \kappa_{1_d}^{(k)}]^\top$  and the  $k$ -th component vector of third-order cumulants by  $\boldsymbol{\kappa}_3^{(k)} = [\kappa_{3_1}^{(k)}, \dots, \kappa_{3_d}^{(k)}]^\top$  for all  $k \in [K]$ . We also define the averages across mixture components,  $\bar{\boldsymbol{\kappa}}_1 = [\bar{\kappa}_{1_1}, \dots, \bar{\kappa}_{1_d}]^\top = \sum_{k=1}^K w^{(k)} \boldsymbol{\kappa}_1^{(k)}$ , and  $\bar{\boldsymbol{\kappa}}_3 = [\bar{\kappa}_{3_1}, \dots, \bar{\kappa}_{3_d}]^\top = \sum_{k=1}^K w^{(k)} \boldsymbol{\kappa}_3^{(k)}$ . Since the  $\tilde{P}_i \forall i \in [d]$  are independently distributed, the  $k$ -th component's  $d \times d$  covariance matrix  $\boldsymbol{\Sigma}^{(k)}$  is diagonal with the  $i$ -th entry  $\kappa_{2_i}^{(k)}$ . The  $d \times d$  mixture covariance matrix is  $\boldsymbol{\Sigma} = \text{E}[(\mathbf{p} - \bar{\boldsymbol{\kappa}}_1)(\mathbf{p} - \bar{\boldsymbol{\kappa}}_1)^\top]$ .

To conclude this section, we formulate the following assumption on the  $p$ -values.

**Assumption 1** (Similar component variances). *The marginal variances of the  $k$ -th mixture component are similar, such that they can be treated as approximately equivalent across the marginals, i.e.,  $\kappa_{2_i}^{(k)} \approx \kappa_{2_i}^{(k)} \forall i \in [d], k \in [K]$ .*

In other words, for a certain  $m \in [M]$ , the entries of  $\mathbf{p}_m$  can be treated as observations of random variables with approximately equivalent variances.

**Proposition 1.** *There exist a subset size  $M < Q$  and a number of mixture components  $K < d$  for which the  $p$ -value subsets  $\mathcal{P}_m^d$  and vectors  $\mathbf{p}_m, m \in [M]$ , can be formed such that Assumption 1 holds for each mixture component  $k \in [K]$ .*

Thus, the  $\mathbf{p}_m, m \in [M]$ , can be divided into  $K$  groups such that joint PDF of the  $p$ -value vectors in each group is described by mixture component  $k$ . For illustration purposes, consider that the subsets  $\mathcal{P}_m^d$  are formed based on spatial proximity, i.e., each  $\mathcal{P}_m^d$  is composed of  $p$ -values from  $d$  neighboring locations. For those subsets containing exclusively  $p$ -values from locations  $q \in \mathcal{H}_0$ , the statistical properties of each element are similar by design. Due to the assumed spatial smoothness of the physical phenomena of interest, also the  $p$ -values obtained at close-by locations  $q \in \mathcal{H}_1$  have similar statistical properties. Our simulation results in Sec. VI confirm that Assumption 1 is fairly mild.

Under Assumption 1, the  $k$ -th mixture component covariance matrix is  $\boldsymbol{\Sigma}^{(k)} \approx \kappa_{2_i}^{(k)} \mathbf{I}_{d \times d}$ , where  $\mathbf{I}_{d \times d}$  is the  $d \times d$  identity matrix. The average variance over mixture components is  $\bar{\kappa}_{2_i} \approx \sum_{k=1}^K w^{(k)} \kappa_{2_i}^{(k)}$ .

### C. The spectral method of moments

The spectral method of moments was formulated for multivariate spherically Gaussian distributed data in [45]. Their approach builds on the relation between the population moments and the model parameters, namely, the

mixture weights, means and variances. In this section, we formulate similar relations for the  $p$ -value vectors, given that they follow the model from Eq. (12) and fulfill Assumption 1. We first extend [45, Theorem 2] such that it fits to our proposed data model.

**Theorem 1** (Relation of mixture model parameters to spectral quantities). *For a  $d \times 1$  random vector  $\mathbf{p}$  with joint PDF  $f_{\mathbf{p}}(\mathbf{p})$  defined in Eq. (12) and under Assumption 1, the beta distribution shape parameters  $a_i^{(k)} \forall i \in [d]$  and mixture component weights  $w^{(k)} \forall k \in [K]$  can be expressed by  $a_i^{(k)} = \frac{\kappa_{1_i}^{(k)}}{1 - \kappa_{1_i}^{(k)}}$  and  $\mathbf{w} = \left[ \kappa_1^{(1)}, \dots, \kappa_1^{(K)} \right]^\dagger \overline{\kappa_1} = \left[ w^{(1)}, \dots, w^{(K)} \right]^\top$  with*

$$\kappa_1^{(k)} = \frac{\lambda^{(k)}}{\boldsymbol{\eta}^\top \mathbf{B} \mathbf{v}^{(k)}} \mathbf{B} \mathbf{v}^{(k)}, \quad (16)$$

if  $K < d$ ,  $w^{(k)} > 0, \forall k \in [K]$  and the  $k$ -th mixture component mean vectors  $\kappa_1^{(k)} \forall k \in [K]$  are linearly independent. Here,  $\boldsymbol{\eta} = [\eta_1, \dots, \eta_d]^\top$  is a vector chosen uniformly at random from the unit sphere in  $\mathbb{R}^d$ ,  $(\lambda^{(k)}, \mathbf{v}^{(k)})$ ,  $k \in [K]$  are the (eigenvalue, eigenvector) pairs of a  $K \times K$  matrix  $\mathbf{W}^\top \mathbf{M}_3(\boldsymbol{\eta}) \mathbf{W}$ . The projection matrices  $\mathbf{B} = \mathbf{U}(\mathbf{U}^\top \mathbf{M}_2 \mathbf{U})^{\frac{1}{2}} \in \mathbb{R}^{K \times d}$  and  $\mathbf{W} = \mathbf{U}(\mathbf{U}^\top \mathbf{M}_2 \mathbf{U})^{\dagger \frac{1}{2}} \in \mathbb{R}^{d \times K}$  are based on the matrix of left singular vectors  $\mathbf{U} \in \mathbb{R}^{d \times K}$  of the thin singular value decomposition (SVD) of  $\mathbf{M}_2 = \mathbf{U} \mathbf{S} \mathbf{R}^\top$ . In addition,  $\mathbf{M}_2, \mathbf{M}_3(\boldsymbol{\eta}) \in \mathbb{R}^{d \times d}$  and  $\underline{\mathbf{M}}_3 \in \mathbb{R}^{d \times d \times d}$  such that

$$\mathbf{M}_2 = \sum_{k=1}^K w^{(k)} \kappa_1^{(k)} \circ \kappa_1^{(k)}, \quad (17)$$

$$\mathbf{M}_3(\boldsymbol{\eta}) = \sum_{i_1=1}^d \sum_{i_2=1}^d \sum_{i_3=1}^d [\underline{\mathbf{M}}_3]_{i_1, i_2, i_3} [\boldsymbol{\eta}]_{i_3} \mathbf{e}_{i_1} \circ \mathbf{e}_{i_2}, \quad (18)$$

$$\underline{\mathbf{M}}_3 = \sum_{k=1}^K (w^{(k)} \kappa_1^{(k)} \circ \kappa_1^{(k)} \circ \kappa_1^{(k)}), \quad (19)$$

with  $\mathbf{e}_i$  a  $d \times 1$  vector of  $d - 1$  zeros and 1 as its  $i$ -th entry.  $\circ$  is the outer product.

*Proof.*  $a_i^{(k)} = \frac{\kappa_{1_i}^{(k)}}{1 - \kappa_{1_i}^{(k)}}$  follows from Eq. (14). The relations for the mixture component means  $\kappa_1^{(k)}$ ,  $k \in [K]$  and the mixture proportion vector  $\mathbf{w}$  result directly from the proof of [45, Theorem 2]. Note, that  $\mathbf{B} \mathbf{B}^\top = \mathbf{M}_2$  and  $\mathbf{W} \mathbf{W}^\top = \mathbf{M}_2^{-1}$ , which implies that  $\mathbf{W}^\top \mathbf{M}_3(\boldsymbol{\eta}) \mathbf{W} = \mathbf{R}^\top \mathbf{D}(\boldsymbol{\eta}) \mathbf{R}$  is diagonalizable along the lines of  $\mathbf{M}_{\text{GMM}}(\boldsymbol{\eta})$  in [45, Theorem 2] by a diagonal matrix  $\mathbf{D}(\boldsymbol{\eta}) \in \mathbb{R}^{K \times K}$  with diagonal entries  $\lambda^{(k)} = \boldsymbol{\eta}^\top \kappa_1^{(k)}$ ,  $k \in [K]$ .  $\square$

The relations established in Theorem 1 allow to estimate the mixture model by means of its parameters  $\kappa_1^{(k)}$  and  $\mathbf{w}$ , since  $\overline{\kappa_1}$ ,  $\mathbf{M}_2$ , and  $\underline{\mathbf{M}}_3$  enable a one-to-one mapping between the model parameters and the observable population moments. In particular,  $\overline{\kappa_1} = \mathbb{E}[\mathbf{p}]$  is the first moment of  $\mathbf{p}$ , whereas  $\mathbf{M}_2$  and  $\underline{\mathbf{M}}_3$  are related to the second and third moments  $\mathbb{E}[\mathbf{p} \circ \mathbf{p}]$  and  $\mathbb{E}[\mathbf{p} \circ \mathbf{p} \circ \mathbf{p}]$  of  $\mathbf{p}$ . The exact relationships are derived in Theorem 2.

**Theorem 2** (Relation of spectral to observable quantities). *Under the assumptions in Theorem 1, the average variance over mixture components  $\overline{\kappa_2} = \sum_{k=1}^K w^{(k)} \kappa_2^{(k)}$  is the smallest eigenvalue of the population covariance*

matrix  $\Sigma$ . With  $\mathbf{v} \in \mathbb{R}^d$  any unit-norm eigenvector of eigenvalue  $\overline{\kappa_2}$ , we find

$$\mathbf{M}_2 = \mathbb{E} [\mathbf{p} \circ \mathbf{p}] - \overline{\kappa_2} \mathbf{I}_{d \times d}, \quad (20)$$

$$\mathbf{M}_3 = \tilde{\mathbf{M}}_3 - \mathbf{M}_3^\Delta, \quad (21)$$

where the observable  $\tilde{\mathbf{M}}_3$  and the difference  $\mathbf{M}_3^\Delta$  to the non-observable  $\mathbf{M}_3$  are

$$\begin{aligned} \tilde{\mathbf{M}}_3 = \mathbb{E} [\mathbf{p} \circ \mathbf{p} \circ \mathbf{p}] - \sum_{i=1}^d (\tilde{\mathbf{m}}_1 \circ \mathbf{e}_i \circ \mathbf{e}_i \\ + \mathbf{e}_i \circ \tilde{\mathbf{m}}_1 \circ \mathbf{e}_i + \mathbf{e}_i \circ \mathbf{e}_i \circ \tilde{\mathbf{m}}_1), \end{aligned} \quad (22)$$

$$\mathbf{M}_3^\Delta = \mathbf{M}_3^{\Delta_3} - \mathbf{M}_3^{\Delta_1}, \quad (23)$$

with third-order tensors  $\tilde{\mathbf{M}}_3, \mathbf{M}_3^{\Delta_3}, \mathbf{M}_3^{\Delta_1} \in \mathbb{R}^{d \times d \times d}$ ,  $d \times 1$  vector  $\tilde{\mathbf{m}}_1 = \mathbf{m}_1 + \mathbf{m}_1^\Delta \in \mathbb{R}^d$ ,

$$\tilde{\mathbf{m}}_1 = \mathbb{E} \left[ \mathbf{p} \left( \mathbf{v}^\top (\mathbf{p} - \overline{\kappa_1}) \right)^2 \right], \quad \mathbf{m}_1^\Delta = \mathbf{v} \odot \mathbf{v} \odot \overline{\kappa_3}. \quad (24)$$

$\odot$  denotes the Hadamard product and

$$\mathbf{M}_3^{\Delta_3} = \sum_{i=1}^d \left( \overline{\kappa_{3_i}} \mathbf{e}_i \circ \mathbf{e}_i \circ \mathbf{e}_i \right) \quad (25)$$

$$\begin{aligned} \mathbf{M}_3^{\Delta_1} = \sum_{i=1}^d \left( \mathbf{m}_1^\Delta \circ \mathbf{e}_i \circ \mathbf{e}_i \right. \\ \left. + \mathbf{e}_i \circ \mathbf{m}_1^\Delta \circ \mathbf{e}_i + \mathbf{e}_i \circ \mathbf{e}_i \circ \mathbf{m}_1^\Delta \right). \end{aligned} \quad (26)$$

$\overline{\kappa_3} = [\overline{\kappa_{3_1}}, \dots, \overline{\kappa_{3_d}}]^\top$  is the vector composed of the  $d$  marginals' mean third cumulants, i.e., Eq. (15)  $\forall i \in [d]$  averaged over the  $K$  mixture components.

*Proof.* See Appendix A. □

The first and second population moments  $\overline{\kappa_1}$  and  $\mathbb{E} [\mathbf{p} \circ \mathbf{p}]$ , the population covariance matrix  $\Sigma$  and consequently also  $\overline{\kappa_2}$ ,  $\mathbf{v}$  and  $\mathbf{M}_2$  can be found using consistent sample estimates of the moments and covariance.  $\mathbf{M}_3(\boldsymbol{\eta})$  cannot be estimated directly, since only  $\tilde{\mathbf{M}}_3$  depends exclusively on sample moments, but not  $\mathbf{M}_3^\Delta$ . However, we show in Appendix B that  $\tilde{\mathbf{M}}_3(\boldsymbol{\eta}) = \sum_{i_1=1}^d \sum_{i_2=1}^d \sum_{i_3=1}^d [\tilde{\mathbf{M}}_3]_{i_1, i_2, i_3} [\boldsymbol{\eta}]_{i_3} \mathbf{e}_{i_1} \circ \mathbf{e}_{i_2}$  is a sufficiently good approximation of  $\mathbf{M}_3(\boldsymbol{\eta})$  for estimating the  $p$ -value mixture density.  $\tilde{\mathbf{M}}_3(\boldsymbol{\eta})$  is observable. In the following section, we exploit these relations to estimate the component first central moments  $\kappa_1^{(k)}$  and the model parameters  $a_i^{(k)}$ ,  $w^{(k)} \forall k \in [K]$ ,  $\forall i \in [d]$  for Eq. (13).

#### D. The lfd-r-sMoM estimator

The proposed method is summarized in Alg. 1. It partitions the  $p$ -values into subsets, estimates the parameters for the joint PDF of the resulting  $p$ -value vectors and determines  $\hat{f}_P(p) = \hat{f}_P^{\text{BM}}(p)$  from Eq. (13). The density fit is repeated several times for different  $p$ -value vectors, increasing subset sizes  $d = 2, 3, \dots$  and increasing model orders  $K < d$ . If the distinct subsets  $\mathcal{P}_m^d \subset \mathcal{P}^Q$  are immovable, because they are formed based on fixed covariate information like spatial proximity, we randomly rearrange the elements within each  $p$ -value vector for different

runs. The lfd $r$ 's are estimated using  $\hat{f}_{\mathcal{P}}(p)$ , Eq. (9) and Eq. (7). The goodness of fit is assessed by the value  $\ell^*$  of a difference measure between  $\hat{f}_{\mathcal{P}}(p)$  and the data.  $\ell^*$  is initialized with a large value, to ensure that the algorithm finds a solution. The best solution has been found, if additional degrees of freedom do not lead to a better fit.

The parameters of the  $p$ -value vector mixture density are estimated by Alg. 2, which determines the right side of Eq. (16) from the sample moments. In Line 1, the data is split into two distinct sets of equal size. If  $M$  is odd, we drop one  $\mathbf{p}_m$ . The sample moment-based estimates  $\hat{\mathbf{M}}_2$  for  $\mathbf{M}_2$  and  $\hat{\mathbf{M}}_3(\boldsymbol{\eta})$  for  $\mathbf{M}_3(\boldsymbol{\eta})$  are multiplied during the estimation process. Hence, they must be computed from different data to guarantee their independence. The sample covariance matrix estimates  $\hat{\boldsymbol{\Sigma}}_S$  in Line 3 are full rank, but Line 5 reduces the rank to its assumed value  $K$ .  $\hat{\mathbf{M}}_3$  is determined in Lines 6 and 7. Lines 8 to 13 are dedicated to the estimation of the eigenvector, eigenvalue pairs  $(\lambda^{(k)}, \mathbf{v}^{(k)})$  for Eq. (16). We generate  $U$  different vectors  $\boldsymbol{\eta}_u$  and select the best run in Alg. 1 to fulfill Lemma 1. We found a value as low as  $U = 10$  to provide satisfying results. The best density fit is determined based on a difference measure  $d(\hat{f}_{\mathcal{P}}^u(p), \text{hist}(\mathcal{P}^Q))$  between model estimates  $\hat{f}_{\mathcal{P}}^u(p)$  and the histogram of the observed data. We ran Alg. 1 with some of the most popular measures for quantifying closeness based on probability densities and distributions. We found Alg. 1 to be robust w.r.t. the selected difference measure in terms of FDR control. We observed that using empirical distribution function (EDF)-based distances such as the WS or Kolmogorov-Smirnov (KS) distance resulted in slightly higher detection power for very small  $\pi_0$  than PDF-based divergences, such as the KL or the Jensen–Shannon (JS) divergence. Thus, we stick to EDF distances.

Our method inherently avoids overfitting. The model order is limited by the number of elements per subset,  $K < d$ . Hence, increasing  $d$  adds flexibility and reduces the mismatch  $\underline{\mathbf{M}}_3^{\Delta}$  between the observable and non-observable theoretical third-order moment dependent terms. Contrarily, increasing  $d$  decreases the validity of Assumption 1, i.e., equal variance among the multivariate mixture components. In addition, an increase in  $d$  reduces the accuracy of the model parameter estimates due to the decrease in sample size  $M = \lfloor Q/d \rfloor$  and increase in the number of parameters to be estimated.

## V. INTERPOLATION OF LOCAL FALSE DISCOVERY RATES

In this section, we discuss how to determine the decision statistics between the spatially sparse sensor locations.

Like in Fig. 3, sensors are typically positioned at a subset of locations  $\{\mathbf{c}_n\}_{n \in N}$ ,  $N \leq Q$ . These report local  $p$ -values  $\mathcal{P}^N = \{p_1, \dots, p_N\}$  to the FC. The FC computes sensor-level lfd $r$  estimates  $\text{lfd}r_n, \forall n \in [N]$  using lfd $r$ -sMoM. Finally, the lfd $r$ 's are interpolated by radial basis function (RBF) interpolation with thin-plate splines (TPS) to estimate the lfd $r$ 's  $\hat{\text{lfd}}r_q$  at locations  $\{\mathbf{c}_q\}$  between sensors,  $N < q \leq Q$ . Finally, the region of interesting behavior is formed with Eq. (6).

RBF interpolation is an advanced mesh-free method to reconstruct an unknown multivariate function from observed data [48], [49]. The function value at a location of interest is calculated as a weighted sum of smooth basis functions whose value depends on the location's distance to the sampling locations. While different types of basis functions exist, we choose to use TPS [50]. They are a popular choice for interpolating spatial phenomena from scattered data [51], since they inherently promote spatially smooth interpolants for two dimensional functions [52]. This fits well to the physics of our problem, as the assumed spatial smoothness of the observed phenomenon

**Algorithm 1** The proposed algorithm lfdr-sMoM**Input:**  $\mathcal{P}^Q = \{p_1, \dots, p_Q\}$ ,  $\mathcal{K}$ ,  $\mathcal{D}$ ,  $G$ ,  $d(\cdot, \cdot)$ ,  $U$ **Output:**  $\hat{\text{lfdr}}_1, \dots, \hat{\text{lfdr}}_Q$ **Step 1:** Estimation of  $f_P(p)$ 

- 1: Initialize  $\ell^*$  as the largest possible number
- 2: Compute the histogram  $\text{hist}(\mathcal{P}^Q)$  for the data in  $\mathcal{P}^Q$
- 3: **for**  $d \in \mathbb{N}_{\geq 2}$  **do**
- 4:     Divide  $\mathcal{P}^Q$  into subsets  $\mathcal{P}_m^d$ ,  $m \in [M]$
- 5:     **for**  $g \in [G]$  **do**
- 6:         Form vectors  $\mathbf{p}_m \in \mathbb{R}^d$ ,  $\forall m \in [M]$ , by random ordering of the elements in  $\mathcal{P}_m^d$
- 7:         Define  $\mathcal{P}^{d \times M} = \{\mathbf{p}_m \in \mathbb{R}^d \mid m \in [M]\}$ ,  $\ell^d = \infty$
- 8:         **for**  $K \leq d$  **do**
- 9:             Obtain  $U$  sets of parameters  $\hat{w}_u^{(k)}$ ,  $\hat{a}_{i,u}^{(k)}$ ,  $\forall k \in [K]$ ,  $\forall i \in [d]$ ,  $\forall u \in [U]$  via Alg. 2
- 10:             Find  $\hat{f}_P^u(p)$  for  $\hat{w}_u^{(k)}$ ,  $\hat{a}_{i,u}^{(k)}$  and Eq. (13)  $u \in [U]$
- 11:             Select  $u^* = \text{argmin}_u (d(\text{hist}(\mathcal{P}^Q), \hat{f}_P^u(p)))$
- 12:             **if**  $d(\text{hist}(\mathcal{P}^Q), \hat{f}_P^{u^*}(p)) < \ell^d$  **then**
- 13:                  $\ell^d = d(\text{hist}(\mathcal{P}^Q), \hat{f}_P^{u^*}(p))$
- 14:                 **if**  $\ell^d \leq \ell^*$  **then**
- 15:                      $\ell^* = \ell^d$ ,  $\hat{f}_P(p) = \hat{f}_P^{u^*}(p)$ ,  $d^* = d$
- 16:             **else break.**
- 17:         **if**  $d^* \neq d$  **then break.**

**Step 2:** Estimation of  $\pi_0$  and  $f_{P|H_1}(p)$ 

- 18: Compute  $\hat{\pi}_0 = \min(\hat{f}_P(p))$
- 19: Compute  $\hat{f}_{P|H_1}(p) = (1 - \hat{\pi}_0)^{-1}(\hat{f}_P(p) - \hat{\pi}_0)$
- 20: Determine  $\hat{\text{lfdr}}_q$ ,  $\forall q \in [Q]$  from Eq. (7)

implies spatial smoothness of the probabilities of null hypothesis and alternative. In addition, TPS RBFs does not require ad-hoc tuning of additional parameters. This would be necessary, if other popular basis functions, such as the Gaussian or multiquadric were used.

The interpolated lfdr's are calculated as

$$\hat{\text{lfdr}}_q = \sum_{n=1}^N \alpha_n \varphi(r_{n,q}), \quad q \in [Q], \quad (27)$$

where  $r_{n,q} = \|\mathbf{c}_n - \mathbf{c}_q\|_2$  is the Euclidean distance between sensor and location,  $\varphi(r_{n,q}) = r_{n,q}^2 \ln(r_{n,q})$  is the TPS RBF and the weights  $\alpha_n \in \mathbb{R}$  are determined based on the estimated sensor lfdr's and locations by solving [49,

**Algorithm 2** Mixture model parameter estimation**Input:**  $\mathcal{P}^{d \times M} = \{\mathbf{p}_m \in \mathbb{R}^d \mid m = 1, \dots, M\}$ ,  $K$ **Output:**  $\hat{\mathbf{w}}_u \in \mathbb{R}^K$ ,  $\hat{a}_{i,u}^{(k)}$ ,  $\forall i \in [d], \forall k \in [K], \forall u \in [U]$ 

- 1: Randomly split  $\mathcal{P}^{d \times M}$  into  $\{\mathcal{Q}, \mathcal{R} \mid |\mathcal{Q}| = |\mathcal{R}|, \mathcal{Q} \cap \mathcal{R} = \emptyset\}$
- 2: Compute  $\hat{\kappa}_{1\mathcal{S}} = |\mathcal{S}|^{-1} \sum_{\mathbf{p} \in \mathcal{S}} \mathbf{p}$ ,  $\mathcal{S} = \mathcal{Q}, \mathcal{R}$
- 3: Find  $\hat{\Sigma}_{\mathcal{S}} = |\mathcal{S}|^{-1} (\sum_{\mathbf{p} \in \mathcal{S}} \mathbf{p} \mathbf{p}^\top) - \hat{\kappa}_{1\mathcal{S}} \hat{\kappa}_{1\mathcal{S}}^\top$ ,  $\mathcal{S} = \mathcal{Q}, \mathcal{R}$
- 4: Determine  $\hat{\kappa}_{2\mathcal{S}}$ , the smallest eigenvalue of  $\hat{\Sigma}_{\mathcal{S}}$  and  $\hat{\mathbf{v}}_{\mathcal{S}}$ , its corresponding eigenvector,  $\mathcal{S} = \mathcal{Q}, \mathcal{R}$
- 5: Compute the best rank- $K$  estimate of  $\mathbf{M}_2$ ,

$$\hat{\mathbf{M}}_2 = \arg \min_{\mathbf{X} \in \mathbb{R}^{d \times d} \mid \text{rank}(\mathbf{X}) \leq K} \|\hat{\Sigma}_{\mathcal{Q}} - \mathbf{X}\|_2.$$

- 6: Find  $\hat{\mathbf{m}}_{1\mathcal{S}} = |\mathcal{S}|^{-1} \sum_{\mathbf{p} \in \mathcal{S}} \mathbf{p} (\hat{\mathbf{v}}_{\mathcal{S}} (\mathbf{p} - \hat{\kappa}_{1\mathcal{S}})^2)$ ,  $\mathcal{S} = \mathcal{Q}, \mathcal{R}$
- 7: Compute  $\hat{\mathbf{M}}_3 = |\mathcal{R}|^{-1} (\sum_{\mathbf{p} \in \mathcal{R}} \mathbf{p} \circ \mathbf{p} \circ \mathbf{p}) - \sum_{i=1}^d (\hat{\mathbf{m}}_{1\mathcal{R}} \circ \mathbf{e}_i \circ \mathbf{e}_i + \mathbf{e}_i \circ \hat{\mathbf{m}}_{1\mathcal{R}} \circ \mathbf{e}_i + \mathbf{e}_i \circ \mathbf{e}_i \circ \hat{\mathbf{m}}_{1\mathcal{R}})$
- 8: Find  $\hat{\mathbf{U}} \in \mathbb{R}^{d \times K}$ , the left singular vectors of  $\hat{\mathbf{M}}_2$
- 9: Compute  $\hat{\mathbf{W}} = \hat{\mathbf{U}} (\hat{\mathbf{U}}^\top \hat{\mathbf{M}}_2 \hat{\mathbf{U}})^{\dagger \frac{1}{2}} \in \mathbb{R}^{d \times K}$  and  $\hat{\mathbf{B}} = \hat{\mathbf{U}} (\hat{\mathbf{U}}^\top \hat{\mathbf{M}}_2 \hat{\mathbf{U}})^{\frac{1}{2}} \in \mathbb{R}^{K \times d}$
- 10: **for**  $u \in [U]$  **do**

- 11:     Select  $\boldsymbol{\eta}_u$  uniformly at random from the  $\mathbb{R}^d$  unit sphere

- 12:     Find  $\hat{\mathbf{W}}^\top \hat{\mathbf{M}}_3(\boldsymbol{\eta}_u) \hat{\mathbf{W}} \in \mathbb{R}^{K \times K} \forall k, l \in [K]$ ,

$$\left[ \hat{\mathbf{W}}^\top \hat{\mathbf{M}}_3(\boldsymbol{\eta}_u) \hat{\mathbf{W}} \right]_{k,l} = \sum_{h,i,j \in [d]} [\hat{\mathbf{W}}]_{h,k} [\hat{\mathbf{W}}]_{i,l} [\boldsymbol{\eta}_u]_j \left[ \hat{\mathbf{M}}_3 \right]_{h,i,j}$$

- 13:     Determine the (eigenvalue, eigenvector) pairs

$$\left( \hat{\lambda}_u^{(k)}, \hat{\mathbf{v}}_u^{(k)} \right), k \in [K], \text{ of } \hat{\mathbf{W}}^\top \hat{\mathbf{M}}_3(\boldsymbol{\eta}_u) \hat{\mathbf{W}}$$

- 14:     Compute  $\hat{\kappa}_1^{(k)} = \left( \boldsymbol{\eta}_u^\top \hat{\mathbf{B}} \hat{\mathbf{v}}_u^{(k)} \right)^{-1} \hat{\lambda}_u^{(k)} \hat{\mathbf{B}} \hat{\mathbf{v}}_u^{(k)}$ ,  $k \in [K]$

- 15:     Determine  $\hat{\mathbf{w}}_u = \left[ \hat{\kappa}_1^{(1)}, \dots, \hat{\kappa}_1^{(K)} \right]^\dagger \hat{\kappa}_{1\mathcal{Q}}$

- 16:     Obtain  $\hat{a}_{i,u}^{(k)} = \frac{\hat{\kappa}_1^{(k)}}{1 - \hat{\kappa}_1^{(k)}}$ ,  $\forall i \in [d], \forall k \in [K]$

## Chapter 7]

$$\begin{bmatrix} \varphi(r_{1,1}) & \cdots & \varphi(r_{1,N}) \\ \vdots & \ddots & \vdots \\ \varphi(r_{N,1}) & \cdots & \varphi(r_{N,N}) \end{bmatrix} \begin{bmatrix} \alpha_1 \\ \vdots \\ \alpha_N \end{bmatrix} + \begin{bmatrix} \beta_1 \\ \vdots \\ \beta_N \end{bmatrix} = \begin{bmatrix} \text{lfdr}_1 \\ \vdots \\ \text{lfdr}_N \end{bmatrix},$$

such that  $\sum_{n=1}^N \beta_n \alpha_n = 0 \forall \beta_n \in \mathbb{R}, n \in [N]$ .

## VI. SIMULATION RESULTS

We evaluate the performance of our proposed method on simulated radio frequency electromagnetic field data. The observed signals are simulated by the nonuniform sampling method from [53], which models the propagation of radio waves in a 2D spatial area with path loss and shadow fading [30]. The observations are subject to additive white Gaussian sensor noise. If the power of the received signal is below the noise floor, this sensor is classified

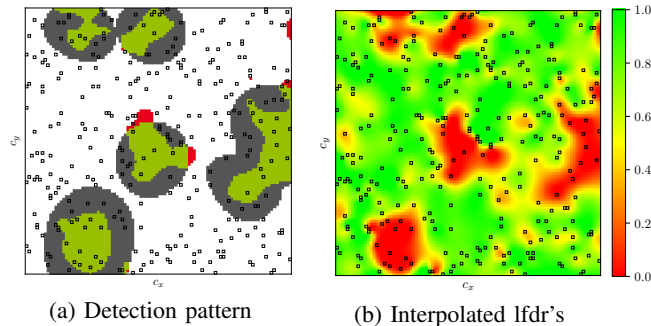


Figure 3: Example for Sc. B, Cnfg. 2. In a), the FDR threshold is set to  $\alpha_{\text{FDR}} = 10\%$ . Green, red and gray indicate true, false and missed discoveries. Boxes mark sensor locations. The interpolated lfdr's of b) are discussed in Sec. VI-C.

as located in the true null region  $\mathcal{H}_0$ . In our simulations, we alter the sensor noise power for different scenarios to obtain different sizes  $|\mathcal{H}_1| = 1 - \pi_0$  of the region of interest.

For simplicity, the sensor  $p$ -values are computed from signal energies. This facilitates the analysis of the results, since its known distributions under null and alternative hypotheses allow for benchmarking the lfdr estimation techniques against the true lfdr's. Also, it offers a simple way to simulate a heterogeneous sensor network by alternating the number of measurements  $T$  at different nodes. In practice, any type of sufficient test statistic could be deployed at the sensor level.

We evaluated our method for a variety of simulated propagating radio wave fields in different environments and sensor network configurations. We discuss results for three scenarios typical for radio frequency sensing. The monitored area is discretized by a grid of  $100 \times 100$  spatial elements for all scenarios and the results are averaged over 200 independent Monte Carlo runs, unless stated otherwise. The sources are placed at random locations, i.e., the fraction  $\pi_0$  of grid points in the null region varies slightly from run to run.

**Sc. A:** Five sources located in a suburban environment covering on average  $1 - \pi_0 \approx 55\%$  of grid points.

**Sc. B:** Eight sources located in a suburban environment covering on average  $1 - \pi_0 \approx 34\%$  of grid points.

**Sc. C:** Two sources in a suburban environment covering on average  $1 - \pi_0 \approx 10\%$  of grid points.

Sc. C is particularly challenging, regardless of the deployed method. Only a small proportion of test statistics provide information on the shape of the alternative component  $f_{P|\mathcal{H}_1}(p)$ .

We investigate three different sensor network configurations.

**Cnfg. 1:**  $N = 10\,000$  identical sensors with  $T = 256$ . Decisions are only made at sensor locations, i.e., no interpolation of decision statistics. This is the classic MHT problem.

**Cnfg. 2:**  $N = 300$  identical sensors with  $T = 256$ , homogeneously distributed across the monitored area. The tests at the sensors are based on local summary statistics, but in between sensors, the lfdr's are interpolated.

**Cnfg. 3:**  $N_1 = 170$  sensors with  $T_1 = 256$ ,  $N = 80$  sensors with  $T_2 = 512$  and  $N_3 = 50$  sensors  $T_3 = 1024$ , all types homogeneously distributed across the monitored area. Decisions in areas between sensors base upon interpolated lfdr's.



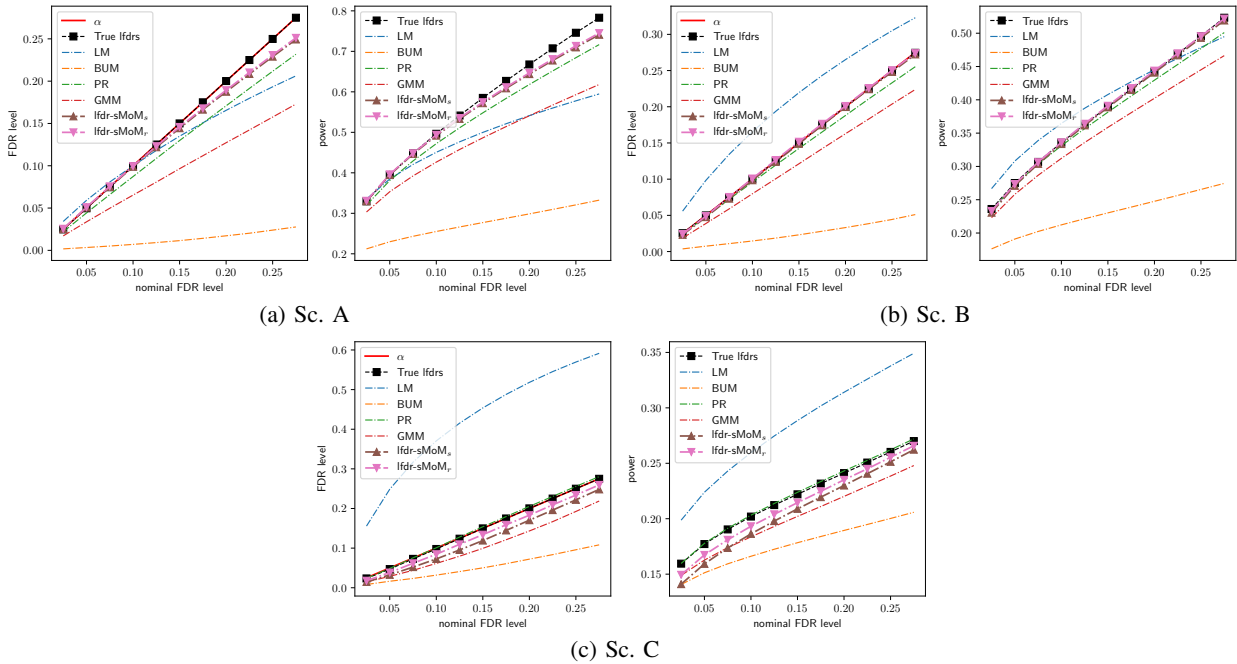


Figure 4: FDR and detection power for all scenarios and a sensor network composed of  $N = 10\,000$  nodes. Inference is only performed at the sensor locations (Cnfg. 1). The FDR is strictly controlled for all scenarios by all methods except LM. Among the FDR controlling methods, ours provides the highest power in Sc. A, B. In Sc. C, where  $\mathcal{H}_1$  contains only a small fraction of all nodes, PR’s power is slightly higher.

**Competitors:** We compare our method to a variety of widely used lfr estimators. We deploy the classic BUM model-based MLE approach from [36]. We also show results obtained with Lindsey’s method (LM) as proposed by Efron [22]. LM which approximates the  $z$ -score PDF by an exponential family model, fitted to the data using Poisson regression. In addition, predictive recursion (PR) [29], [40] is applied, which computes the alternative  $z$ -score PDF by estimating the density of the mean shift of  $z$ -scores from locations in  $\mathcal{H}_1$ . Predictive recursion has recently [23], [26], [39] gained considerable attention in lfr estimation, due to its high accuracy and comparably low computation time. Our implementation of PR follows [26, Appendix A]. Finally, we include a standard Gaussian mixture model (GMM). We do not consider methods whose computational complexity prevents scaling to large-scale sensor networks, as kernel density lfr estimators [38].

#### A. The classic multiple hypothesis testing problem

The results for Cnfg. 1 are shown in Fig. 4. LM faces stability issues due to the heavy one-sided tail of  $f_Z(z)$  when the relative size of the true null region  $\pi_0 = |\mathcal{H}_0|/N$  increases. All other applied methods meet the nominal FDR level for all scenarios. We benchmark by the detection results obtained when using the (in practice unknown) true lfr’s. A higher detection than with the true lfr’s can only be achieved, if the respective method violates the nominal FDR level. For our proposed method, we show results for two variants. For lfr-sMoM<sub>s</sub>, the  $p$ -value vectors are formed by subdividing the grid into square tiles of spatially close grid points. For lfr-sMoM<sub>r</sub>, the  $\{p_n\}_{n \in [N]}$

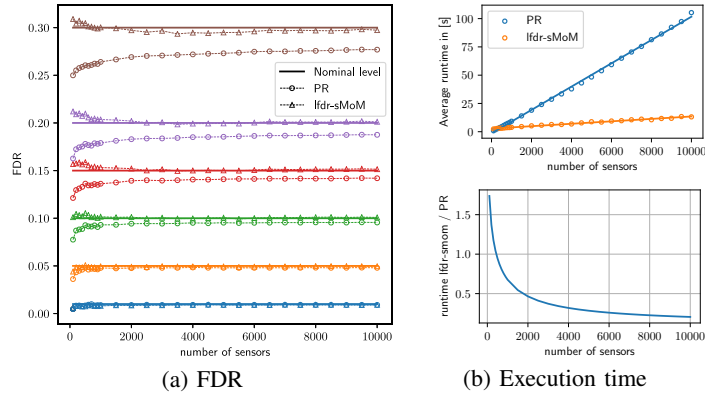


Figure 5: FDRs and run times with increasing sensor network size for lfdr-sMoM vs. the best competitor (PR).

are randomly partitioned into subsets.

The results underline that our proposed multivariate  $p$ -value vector probability density model is very flexible. Even if the  $p$ -value subsets are formed at random, the method finds a parametrization such that the individual components have equal variance (Proposition 1). This confirms that Assumption 1 can be relaxed in practice. For the remainder of this Section, we stick to the conceptually simpler random partitioning and label results obtained with randomly formed  $p$ -value vectors by *lfdr-sMoM*.

The traditional BUM method controls the FDR, but exhibits a low detection power in all scenarios, as does GMM for larger interesting regions. PR performs best by a small margin when the relative size of the alternative region is very small (Sc. C), but our proposed method achieves the largest detection power in Sc. A and Sc. B. Thus, lfdr-sMoM provided the best or very close to the best results in all of the considered scenarios.

### B. Computational demands as the network size increases

In Fig. 5, we compare the best competitor, PR, to our proposed method for different sizes of the sensor network  $N$  and 1000 Monte Carlo (MC) runs. We obtained almost identical results for all scenarios and hence show only those for Sc. B. Again, inference is only performed at the sensor locations. Both, our method and PR, are subject to transient effects when the number of nodes is small. This was to be expected, as fitting a heavy-tailed distribution with such a low number of data points is challenging. Yet, the obtained FDRs are close to the nominal level also for the smallest considered network sizes  $N$ . As  $N$  grows, the nominal and empirical FDR for lfdr-sMoM coincides almost perfectly. Hence, lfdr-sMoM is more efficient in exploiting all permitted false positives than PR, which results in a larger detection power (plot not shown). The comparison of the average execution time per Monte Carlo run in Fig. 5b illustrates, that our method is considerably faster than PR as  $N$  increases. The upper plot shows that the execution time for both methods grows approximately linearly. For a small number of sensors, the runtimes of lfdr-sMoM and PR are almost identical, but our method scales significantly better for larger sensor networks. At  $N = 10000$ , lfdr-sMoM is more than five times faster. Both methods were run in Python 3.8.3 on an AMD Ryzen 9 3900X 12-Core CPU.

Table I: Sc. B in Cnfg. 2. The columns indicate different nominal FDR levels. The similarity in the empirical values of FDR and detection power obtained when using lfdr-sMoM or in practice the unavailable true lfdr's as base for the interpolation underline the effectiveness of our method.

	$\alpha_{\text{FDR}}$	.01	.05	.1	.15	.2	.25	.3
FDR	<i>True</i>	.020	.030	.05	.08	.12	.17	.22
	lfdr-sMoM	.029	.043	.07	.10	.15	.19	.24
Power	<i>True</i>	.10	.18	.25	.33	.40	.47	.55
	lfdr-sMoM	.11	.19	.26	.34	.41	.48	.55

Table II: Sc. B in Cnfg. 3. The columns indicate different nominal FDR levels. Also for a heterogeneous sensor network, the FDR is controlled except for the very small  $\alpha_{\text{FDR}} = .01$ .

	$\alpha_{\text{FDR}}$	.01	.05	.1	.15	.2	.25	.3
FDR	lfdr-sMoM	.023	.039	.07	.11	.15	.20	.25
Power	lfdr-sMoM	.15	.24	.33	.42	.49	.56	.63

While lfdr-sMoM often provides the highest detection power, it also outperforms its strongest competitor significantly in terms of computation time for growing  $N$ . Lfdr-sMoM is the best fit for large-scale sensor networks.

### C. Spatial interpolation of lfdr's

It is of high interest to find the boundaries of the regions associated with interesting, anomalous or different behavior. The lfdr values between the sensor locations can be determined through spatial interpolation. This allows for segmenting the observation area into  $\mathcal{H}_0$  and  $\mathcal{H}_1$ .

An exemplary map of interpolated lfdr's with  $N = 300$  identical sensors (Cnfg. 2), is shown in Fig. 3, along the detection pattern for the most commonly used [22] nominal FDR level  $\alpha_{\text{FDR}} = 0.1$ . In Tab. I, we present the numerical FDRs and detection powers obtained by interpolating the estimated sensor lfdr's. Note, that interpolating the lfdr's is a novel approach and could also be combined with any existing lfdr estimator, such as PR.

The FDR is controlled at the nominal level, except for the very small  $\alpha_{\text{FDR}} = 0.01$ . This nominal level is so small, that even the slightest interpolation error can lead to its violation. In this example, lfdr's are computed at only 3% of all grid points, and interpolated at the remaining 97%. These results strongly indicate that the interpolation of lfdr's is a powerful tool to decide between  $\mathcal{H}_0$  and  $\mathcal{H}_1$  at locations where no sensor is present and local summary statistics are not available.

In Cnfg. 3, we considered a heterogeneous sensor network composed of multiple types of sensors with different individual detection capabilities due to varying sensor noise levels. The results in Tab. II verify the applicability of our method to heterogeneous sensor networks, i.e., to accommodate various types of sensors into the inference process.

## VII. THE INCLUSION OF DOMAIN-SPECIFIC KNOWLEDGE

While we kept this work general to maintain its applicability to a wide area of practical problems, extending the procedure to explicitly account for the particular nature of the observed physical phenomenon, such as electromagnetic spectrum, air quality or agricultural fields appears promising. This could further increase the detection power. One could plug in an novel or existing method [23], [24] to replace the constant  $\pi_0$  by a suitable spatially varying prior in Eq. (5) when calculating the sensor lfders. Also, RBF interpolation allows to include a penalty to spatially smooth the interpolant [48]. Choosing the value of this parameter is non-trivial and should be done in an application-dependent manner.

## VIII. SUMMARY

We proposed a general spatial inference method for detecting interesting, different or anomalous regions for an observed physical phenomenon. Our approach provides statistical performance guarantees in terms of false positives. The proposed method facilitates solving real-world spatial inference problems in which distributed heterogeneous large-scale sensor networks observe spatial phenomena. A prime example is IoT. It is considerably faster than state-of-the-art methods. The sensors communicate with a fusion center or cloud only in a limited fashion. This saves battery and ensures a long sensor life-span. Our individual contributions are as follows. We formulated the problem using a large-scale multiple hypothesis framework where the false discovery rate is controlled. We developed a novel method to compute local false discovery rates in a data-driven fashion based on quantities estimated with the spectral method of moments. It outperforms existing methods in terms of detection power and runtime in a variety of scenarios. We proposed a method for interpolating local false discovery rate values at locations where no sensor is present. This allows for identifying regions associated with null hypothesis and alternative, as well as estimating their boundaries. The performance was evaluated by an application to spatially varying radio frequency waves. The code to reproduce the results is available on <https://github.com/mgoelz95/lfd-r-sMoM>.

## APPENDIX A

### PROOF OF THEOREM 2

We establish the one-to-one relations between the first three population moments  $E[\mathbf{p}]$ ,  $E[\mathbf{p} \circ \mathbf{p}]$ ,  $E[\mathbf{p} \circ \mathbf{p} \circ \mathbf{p}]$  and the model parameter-dependent operators  $\mathbf{M}_2 \in \mathbb{R}^{d \times d}$ ,  $\mathbf{M}_3 \in \mathbb{R}^{d \times d \times d}$ , which are given in Eq. (20) and Eq. (21). Since the sample moments are consistent estimates of the population moments, Theorem 1 enables model parameter estimation based on the sample moments.

#### A. Proof of Eq. (20)

Under Assumption 1 with  $d > K$ , the  $d - (K - 1)$  smallest eigenvalues of covariance matrix  $\Sigma \in \mathbb{R}^{d \times d}$  with  $\text{rank}(\Sigma) = \min(K, d) - 1$ ,

$$\begin{aligned} \Sigma &= E[(\mathbf{p} - \bar{\kappa}_1) \circ (\mathbf{p} - \bar{\kappa}_1)] \\ &= \bar{\kappa}_2 \mathbf{I}_{d \times d} + \sum_{k=1}^K w^{(k)} \left( \kappa_1^{(k)} - \bar{\kappa}_1 \right) \circ \left( \kappa_1^{(k)} - \bar{\kappa}_1 \right), \end{aligned} \quad (28)$$

are all equal to  $\overline{\kappa_2}$ .  $\mathbf{v} \in \mathbb{R}^d$  is any of the unit norm eigenvectors corresponding to  $\overline{\kappa_2}$ . The derivation for Eq. (28) in the proof of [45, Theorem 1] applies also to our data model. Thus, also

$$\mathbf{M}_2 = \mathbb{E}[\mathbf{p} \circ \mathbf{p}] - \overline{\kappa_2} \mathbf{I}_{d \times d} = \sum_{k=1}^K w^{(k)} \boldsymbol{\kappa}_1^{(k)} \circ \boldsymbol{\kappa}_1^{(k)}$$

holds and relates the observable second population moment  $\mathbb{E}[\mathbf{p} \circ \mathbf{p}]$  to the model parameters.

### B. Proof of Eq. (21)

We now proof the relation  $\underline{\mathbf{M}}_3 = \tilde{\underline{\mathbf{M}}}_3 - \underline{\mathbf{M}}_3^\Delta$  between the observable  $\tilde{\underline{\mathbf{M}}}_3$  and non-observable  $\underline{\mathbf{M}}_3$ . Random vector  $\mathbf{p} \in \mathbb{R}^d$  is assumed to follow a  $d$ -variate,  $K$ -component mixture model. It can hence be described by  $\mathbf{p} = \mathbf{p}^{(k)}$ , where  $k \in [K]$  is a discrete random variable for the mixture component index taking value  $k = k$  with probability  $w^{(k)} \in [0, 1]$  and  $\sum_{k=1}^K w^{(k)} = 1$ . Let  $\mathbf{q}^{(k)} = \mathbf{p}^{(k)} - \boldsymbol{\kappa}_1^{(k)}$  denote the centered data random vector and conditioned on  $k = k$ ,  $\mathbf{q}^{(k)} = \mathbf{p}^{(k)} - \boldsymbol{\kappa}_1^{(k)}$ . This implies  $\mathbb{E}[\mathbf{q}^{(k)}] = \mathbf{0}_d$ . Since  $\mathbf{q} \in \mathbb{R}^d$ , its  $i$ -th marginal is  $q_i^{(k)}$ ,  $i \in [d]$ , and the marginal variances are  $\mathbb{E}[q_i^{(k)2}] = \kappa_2^{(k)} \forall k \in [K]$  under Assumption 1. The third order central moments are  $\mathbb{E}[q_i^{(k)3}] = \kappa_{3_i}^{(k)}$ .

The third order population moment tensor  $\mathbb{E}[\mathbf{p} \circ \mathbf{p} \circ \mathbf{p}]$  is

$$\begin{aligned} & \mathbb{E}[\mathbf{p} \circ \mathbf{p} \circ \mathbf{p}] \\ &= \sum_{k=1}^K w^{(k)} \left( \mathbb{E} \left[ \left( \boldsymbol{\kappa}_1^{(k)} + \mathbf{q}^{(k)} \right) \circ \left( \boldsymbol{\kappa}_1^{(k)} + \mathbf{q}^{(k)} \right) \circ \left( \boldsymbol{\kappa}_1^{(k)} + \mathbf{q}^{(k)} \right) \right] \right) \\ &= \sum_{k=1}^K w^{(k)} \left( \mathbb{E} \left[ \boldsymbol{\kappa}_1^{(k)} \circ \boldsymbol{\kappa}_1^{(k)} \circ \boldsymbol{\kappa}_1^{(k)} \right] + \mathbb{E} \left[ \boldsymbol{\kappa}_1^{(k)} \circ \mathbf{q}^{(k)} \circ \mathbf{q}^{(k)} \right] \right. \\ & \quad + \mathbb{E} \left[ \mathbf{q}^{(k)} \circ \boldsymbol{\kappa}_1^{(k)} \circ \mathbf{q}^{(k)} \right] + \mathbb{E} \left[ \mathbf{q}^{(k)} \circ \mathbf{q}^{(k)} \circ \boldsymbol{\kappa}_1^{(k)} \right] \\ & \quad \left. + \mathbb{E} \left[ \mathbf{q}^{(k)} \circ \mathbf{q}^{(k)} \circ \mathbf{q}^{(k)} \right] \right) \\ &= \sum_{k=1}^K w^{(k)} \left( \boldsymbol{\kappa}_1^{(k)} \circ \boldsymbol{\kappa}_1^{(k)} \circ \boldsymbol{\kappa}_1^{(k)} + \sum_{i=1}^d \left( \boldsymbol{\kappa}_1^{(k)} \kappa_2^{(k)} \circ \mathbf{e}_i \circ \mathbf{e}_i \right. \right. \\ & \quad + \mathbf{e}_i \circ \boldsymbol{\kappa}_1^{(k)} \kappa_2^{(k)} \circ \mathbf{e}_i + \mathbf{e}_i \circ \mathbf{e}_i \circ \boldsymbol{\kappa}_1^{(k)} \kappa_2^{(k)} \\ & \quad \left. \left. + \kappa_{3_i}^{(k)} \mathbf{e}_i \circ \mathbf{e}_i \circ \mathbf{e}_i \right) \right) \\ &= \underline{\mathbf{M}}_3 + \underline{\mathbf{M}}_3^\Delta + \sum_{i=1}^d \left( \sum_{k=1}^K w^{(k)} \left( \boldsymbol{\kappa}_1^{(k)} \kappa_2^{(k)} \circ \mathbf{e}_i \circ \mathbf{e}_i \right. \right. \\ & \quad \left. \left. + \mathbf{e}_i \circ \boldsymbol{\kappa}_1^{(k)} \kappa_2^{(k)} \circ \mathbf{e}_i + \mathbf{e}_i \circ \mathbf{e}_i \circ \boldsymbol{\kappa}_1^{(k)} \kappa_2^{(k)} \right) \right). \end{aligned} \tag{29}$$

The definitions of  $\tilde{\mathbf{M}}_3, \mathbf{M}_3^{\Delta_3} \in \mathbb{R}^{d \times d \times d}$  are provided in Eq. (19) and Eq. (25). We proceed with  $\tilde{\mathbf{m}}_1 \in \mathbb{R}^d$ ,

$$\begin{aligned}
\tilde{\mathbf{m}}_1 &= \mathbb{E} \left[ \mathbf{p} \left( \mathbf{v}^\top (\mathbf{p} - \overline{\boldsymbol{\kappa}}_1) \right)^2 \right] \\
&= \sum_{k=1}^K w^{(k)} \mathbb{E} \left[ \mathbf{p}^{(k)} \left( \mathbf{v}^\top (\mathbf{p}^{(k)} - \overline{\boldsymbol{\kappa}}_1) \right)^2 \right] \\
&= \sum_{k=1}^K w^{(k)} \mathbb{E} \left[ \left( \boldsymbol{\kappa}_1^{(k)} + \mathbf{q}^{(k)} \right) \left( \mathbf{v}^\top \left( \boldsymbol{\kappa}_1^{(k)} - \overline{\boldsymbol{\kappa}}_1 + \mathbf{q}^{(k)} \right) \right)^2 \right] \\
&= \sum_{k=1}^K w^{(k)} \mathbb{E} \left[ \left( \boldsymbol{\kappa}_1^{(k)} + \mathbf{q}^{(k)} \right) \left( \mathbf{v}^\top \mathbf{q}^{(k)} \right)^2 \right] \\
&= \sum_{k=1}^K w^{(k)} \left( \mathbb{E} \left[ \boldsymbol{\kappa}_1^{(k)} \left( \mathbf{v}^\top \mathbf{q}^{(k)} \right)^2 \right] + \mathbb{E} \left[ \mathbf{q}^{(k)} \left( \mathbf{v}^\top \mathbf{q}^{(k)} \right)^2 \right] \right) \\
&= \sum_{k=1}^K w^{(k)} \left( \boldsymbol{\kappa}_1^{(k)} \boldsymbol{\kappa}_2^{(k)} + \mathbf{v} \odot \mathbf{v} \odot \boldsymbol{\kappa}_3^{(k)} \right). \tag{30}
\end{aligned}$$

The transition from line 3 to 4 in Eq. (30) uses the property that  $\mathbf{v}$  lies in the null space of  $w^{(k)} \left( \boldsymbol{\kappa}_1^{(k)} - \overline{\boldsymbol{\kappa}}_1 \right) \odot \left( \boldsymbol{\kappa}_1^{(k)} - \overline{\boldsymbol{\kappa}}_1 \right)$ . With  $\mathbb{E} \left[ q_{i_1}^{(k)} q_{i_2}^{(k)} \right] = 0$  if  $i_1 \neq i_2$  due to the diagonal covariance matrix, the first addend in line 6 follows from line 5 by

$$\begin{aligned}
\mathbb{E} \left[ \boldsymbol{\kappa}_1^{(k)} \left( \mathbf{v}^\top \mathbf{q}^{(k)} \right)^2 \right] &= \boldsymbol{\kappa}_1^{(k)} \left( \mathbb{E} \left[ \sum_{i=1}^d \left( v_i^2 q_i^{(k)2} \right) \right] \right) \\
&\quad + \sum_{i_1=1}^d \sum_{i_2=i_1+1}^d 2 \mathbb{E} \left[ q_{i_1}^{(k)} q_{i_2}^{(k)} \right] v_{i_1} v_{i_2}.
\end{aligned}$$

For the second addend in Eq. (30),

$$\begin{aligned}
&= \boldsymbol{\kappa}_1^{(k)} \sum_{i=1}^d v_i^2 \mathbb{E} \left[ q_i^{(k)2} \right] = \boldsymbol{\kappa}_1^{(k)} \sum_{i=1}^d v_i^2 \boldsymbol{\kappa}_2^{(k)} = \boldsymbol{\kappa}_1^{(k)} \boldsymbol{\kappa}_2^{(k)}, \\
\mathbb{E} \left[ \mathbf{q}^{(k)} \left( \mathbf{v}^\top \mathbf{q}^{(k)} \right)^2 \right] &= \mathbb{E} \left[ \mathbf{q}^{(k)} \sum_{i=1}^d \left( v_i^2 q_i^{(k)2} \right) \right] \\
&\quad + \mathbb{E} \left[ \mathbf{q}^{(k)} \sum_{i_1=1}^d \sum_{i_2=i_1+1}^d \left( 2q_{i_1}^{(k)} q_{i_2}^{(k)} v_{i_1} v_{i_2} \right) \right].
\end{aligned}$$

For the  $j$ -th entry,  $j \in [d]$ , of vector  $\mathbb{E} \left[ \mathbf{q}^{(k)} \left( \mathbf{v}^\top \mathbf{q}^{(k)} \right)^2 \right]$ ,

$$\begin{aligned}
\mathbb{E} \left[ q_j^{(k)} \sum_{i=1}^d \left( v_i^2 q_i^{(k)2} \right) \right] &= \mathbb{E} \left[ q_j^{(k)} \left( v_j^2 q_j^{(k)2} \right) \right] = v_j^2 \mathbb{E} \left[ q_j^{(k)3} \right], \\
\mathbb{E} \left[ q_j^{(k)} \sum_{i_1=1}^d \sum_{i_2=i_1+1}^d \left( 2q_{i_1}^{(k)} q_{i_2}^{(k)} v_{i_1} v_{i_2} \right) \right] &= 0,
\end{aligned}$$

and since  $\mathbb{E} \left[ q_j^{(k)3} \right] = \boldsymbol{\kappa}_{3_j}^{(k)}$ ,

$$\mathbb{E} \left[ \mathbf{q} \left( \mathbf{v}^\top \mathbf{q} \right)^2 \right] = \mathbf{v} \odot \mathbf{v} \odot \boldsymbol{\kappa}_3^{(k)}.$$

The proof is concluded by subtracting  $\tilde{\mathbf{m}}_1$  as in Eq. (30) from  $E[\mathbf{p} \circ \mathbf{p} \circ \mathbf{p}]$  in Eq. (29), which results in Eq. (21) when inserting  $\underline{\mathbf{M}}_3^{\Delta_1} \in \mathbb{R}^{d \times d \times d}$  for  $\sum_{i=1}^d \mathbf{m}_1^{\Delta} \circ \mathbf{e}_i \circ \mathbf{e}_i + \mathbf{e}_i \circ \mathbf{m}_1^{\Delta} \circ \mathbf{e}_i + \mathbf{e}_i \circ \mathbf{e}_i \circ \mathbf{m}_1^{\Delta}$  with  $\mathbf{m}_1^{\Delta} := \sum_{k=1}^K \mathbf{v} \odot \mathbf{v} \odot \boldsymbol{\kappa}_3^{(k)}$ .

## APPENDIX B

### APPROXIMATION OF THE THIRD ORDER MOMENT

In this section, we demonstrate that approximating the non-observable  $\mathbf{M}_3(\boldsymbol{\eta})$  by the observable  $\tilde{\mathbf{M}}_3(\boldsymbol{\eta}) \in \mathbb{R}^{d \times d}$  is accurate up to an approximation error  $\tilde{\mathbf{M}}_3(\boldsymbol{\eta}) - \mathbf{M}_3(\boldsymbol{\eta})$ , which is negligible under certain conditions. By definition,

$$\begin{aligned} \tilde{\mathbf{M}}_3(\boldsymbol{\eta}) &= \sum_{i=1}^d \sum_{j=1}^d \sum_{h=1}^d [\tilde{\mathbf{M}}_3]_{i,j,h} \eta_h \mathbf{e}_i \circ \mathbf{e}_j \\ &= \sum_{i=1}^d \sum_{j=1}^d \sum_{h=1}^d \left( [\mathbf{M}_3]_{i,j,h} + [\underline{\mathbf{M}}_3^{\Delta}]_{i,j,h} \right) \eta_j \mathbf{e}_i \circ \mathbf{e}_j. \end{aligned}$$

The entries are thus  $[\tilde{\mathbf{M}}_3(\boldsymbol{\eta})]_{i,j} = \sum_{h=1}^d [\mathbf{M}_3]_{i,j,h} \eta_h + \sum_{h=1}^d [\underline{\mathbf{M}}_3^{\Delta}]_{i,j,h} \eta_h \forall i, j \in [d]$ . If the value of the second sum is small  $\forall i, j \in [d]$ , we can conclude  $\tilde{\mathbf{M}}_3(\boldsymbol{\eta}) \approx \mathbf{M}_3(\boldsymbol{\eta})$ . With Theorem 2, the entries of  $\underline{\mathbf{M}}_3^{\Delta}$  are found to be

$$[\underline{\mathbf{M}}_3^{\Delta}]_{i,j,h} = \begin{cases} (-3v_i^2 + 1)\overline{\kappa_{3_i}} & i = j = h, \\ -v_i^2 \overline{\kappa_{3_i}} & i \neq j = h, \\ -v_j^2 \overline{\kappa_{3_j}} & i = h \neq j, \\ -v_h^2 \overline{\kappa_{3_h}} & i = j \neq h, \\ 0 & i \neq j \neq h. \end{cases}$$

Consequently, the element-wise error between  $\tilde{\mathbf{M}}_3$  and  $\mathbf{M}_3$  is

$$\begin{aligned} [\tilde{\mathbf{M}}_3(\boldsymbol{\eta}) - \mathbf{M}_3(\boldsymbol{\eta})]_{i,j} &= \eta_i \overline{\kappa_{3_i}} - 2\eta_i v_i^2 \overline{\kappa_{3_i}} - \sum_{h=1}^d \eta_h v_h^2 \overline{\kappa_{3_h}} \\ &= \eta_i \left( 1 - 2v_i^2 \right) \overline{\kappa_{3_i}} - \sum_{h=1}^d \eta_h v_h^2 \overline{\kappa_{3_h}} \end{aligned}$$

if row index  $i$  and column index  $j$  are equivalent,  $i = j$ , and

$$[\tilde{\mathbf{M}}_3(\boldsymbol{\eta}) - \mathbf{M}_3(\boldsymbol{\eta})]_{i,j} = -\eta_j v_i^2 \overline{\kappa_{3_i}} - \eta_i v_j^2 \overline{\kappa_{3_j}}$$

if  $i \neq j, \forall i, j \in [d]$ .

Recall the average third cumulant  $\overline{\kappa_{3_i}} = \sum_{k=1}^K w^{(k)} \kappa_{3_i}^{(k)}$ , with  $\kappa_{3_i}^{(k)}$  from Eq. (15).  $-0.0075 < \overline{\kappa_{3_i}} < 0.2222$ , i.e.,  $\overline{\kappa_{3_i}}$  is bounded from below and above. By definition,  $|\mathbf{v}|^2 = \sum_{i=1}^d v_i^2 = 1$ , which implies  $v_i^2 \leq 1 \forall i \in [d]$ .

**Lemma 1.** *Let  $\boldsymbol{\eta} \in \mathbb{R}^d$  be distributed uniformly on the unit sphere in  $\mathbb{R}^d$ , which holds if its  $i$ -th element is  $\eta_i = \frac{x_i}{\sqrt{x_1^2 + \dots + x_d^2}}$  with  $x_i \sim \mathcal{N}(0, 1) \forall i \in [d]$ . For large  $d$ , the  $\eta_i$  become approximately i.i.d. Gaussian distributed,  $\eta_i \sim \mathcal{N}(0, d^{-1})$ . If we generate  $U$  samples of  $\boldsymbol{\eta}$ , we will find an observation  $\boldsymbol{\eta}^*$  such that the errors  $[\tilde{\mathbf{M}}_3(\boldsymbol{\eta}) - \mathbf{M}_3(\boldsymbol{\eta})]_{i,j}$  become arbitrarily small  $\forall i, j \in [d]$  as  $U \rightarrow \infty$ .*

*Proof.* The assumption of i.i.d. Gaussianity of the  $\eta_i \forall i \in [d]$  for large  $d$  is justified by the law of large numbers, since  $d^{-1}(x_1^2 + \dots + x_d^2) \rightarrow 1$  for  $d \rightarrow \infty$ . For the second part of the Lemma, we first assume that all  $d$  entries  $v_i$  are non-zero. Consequently, the fraction of the total mass  $\sum_{i=1}^d v_i^2 = 1$  allocated to an individual entry  $v_i^2$  decreases with increasing  $d$  and the Lemma follows since  $E[\eta_i] = 0$  and  $E[\eta_i^2] = d^{-1} \forall i \in [d]$ . Assume now the opposite case, i.e., the mass  $\sum_{i=1}^d v_i^2 = 1$  is concentrated in a few  $i \in [\tilde{d}]$ ,  $\tilde{d} \ll d$ . Then,  $\sum_{h=1}^d \eta_h v_h^2 \overline{\kappa_{3h}} = \sum_{h=1}^{\tilde{d}} \eta_h v_h^2 \overline{\kappa_{3h}} \sim \mathcal{N}\left(0, d^{-1} \sum_{h=1}^{\tilde{d}} (v_h^2 \overline{\kappa_{3h}})^2\right)$  due to the summation of normally distributed random variables and since  $\sum_{h=1}^{\tilde{d}} v_h^2 \overline{\kappa_{3h}} \ll \tilde{d}$ , the claim of the Lemma follows.  $\square$

In practice, small but non-zero  $[\tilde{\mathbf{M}}_3(\boldsymbol{\eta}) - \mathbf{M}_3(\boldsymbol{\eta})]_{i,j} \forall i, j \in [d]$  are sufficient. To this end, observe that the impact of a non-zero approximation error also depends on the true value of the mixture model parameters, since they determine the model error's *relative* magnitude. In addition, the theoretical  $\tilde{\mathbf{M}}_3$  has to be estimated from the data based on sample moments, which introduces an additional non-zero empirical error. This error often has a larger influence on the results than the mismatch between  $\hat{\tilde{\mathbf{M}}}_3(\boldsymbol{\eta})$  and  $\mathbf{M}_3(\boldsymbol{\eta})$ .

In our proposed method, we account for Lemma 1 by making  $d$  a tuning parameter whose value is chosen such that the resulting  $p$ -value mixture PDF  $\hat{f}_P(p)$  is close to the data. Our simulation results underline that even for small  $U$  and  $d$ , using  $\tilde{\mathbf{M}}_3(\boldsymbol{\eta})$  instead of  $\mathbf{M}_3(\boldsymbol{\eta})$  is reasonable to enable lfr estimation by the spectral method of moments.

## REFERENCES

- [1] E. Arias-de-Reyna, P. Closas, D. Dardari, and P. M. Djuric, "Crowd-based learning of spatial fields for the internet of things: From harvesting of data to inference," *IEEE Signal Process. Mag.*, vol. 35, no. 5, pp. 130–139, Sep. 2018.
- [2] R. Nowak and U. Mitra, "Boundary estimation in sensor networks: Theory and methods," in *Information Processing in Sensor Networks*, Berlin, Heidelberg: Springer Berlin Heidelberg, 2003, pp. 80–95.
- [3] X. Wang, G. Li, and P. K. Varshney, "Detection of sparse signals in sensor networks via locally most powerful tests," *IEEE Signal Process. Lett.*, vol. 25, no. 9, pp. 1418–1422, Sep. 2018.
- [4] E. Nitzan, T. Halme, and V. Koivunen, "Bayesian methods for multiple change-point detection with reduced communication," *IEEE Trans. Signal Process.*, vol. 68, pp. 4871–4886, 2020.
- [5] V. V. Veeravalli and P. K. Varshney, "Distributed inference in wireless sensor networks," *Philos. Trans. Roy. Soc. A Math. Phys. Eng. Sci.*, vol. 370, no. 1958, pp. 100–117, 2012.
- [6] J. W. Tukey, "The philosophy of multiple comparisons," *Statist. Sci.*, vol. 6, no. 1, pp. 100–116, Feb. 1991.
- [7] B. Soric, "Statistical "discoveries" and effect-size estimation," *J. Amer. Statist. Assoc.*, vol. 84, no. 406, pp. 608–610, 1989.
- [8] Y. Benjamini and Y. Hochberg, "Controlling the false discovery rate: A practical and powerful approach to multiple testing," *J. Roy. Statist. Soc. Ser. B*, vol. 57, no. 1, pp. 289–300, 1995.
- [9] A. Zoubir and J. Böhme, "Bootstrap multiple tests applied to sensor location," *IEEE Trans. Signal Process.*, vol. 43, no. 6, pp. 1386–1396, Jun. 1995.
- [10] Y. Benjamini and R. Heller, "False discovery rates for spatial signals," *J. Amer. Statist. Assoc.*, vol. 102, no. 480, pp. 1272–1281, 2007.
- [11] R. F. Barber and A. Ramdas, "The p-filter: Multi-layer fdr control for grouped hypotheses," *J. Roy. Statist. Soc. Ser. B*, vol. 79, no. 4, pp. 1247–1268, Dec. 10, 2015.
- [12] A. Chouldechova, "False discovery rate control for spatial data," Ph.D. dissertation, Stanford University, 2014.
- [13] J. R. Chumbley and K. J. Friston, "False discovery rate revisited: FDR and topological inference using gaussian random fields," *NeuroImage*, vol. 44, no. 1, pp. 62–70, Jan. 2009.
- [14] J. Chumbley, K. Worsley, G. Flandin, and K. Friston, "Topological FDR for neuroimaging," *NeuroImage*, vol. 49, no. 4, pp. 3057–3064, Feb. 2010.



- [15] A. Schwartzman and F. Telschow, "Peak p-values and false discovery rate inference in neuroimaging," *NeuroImage*, vol. 197, pp. 402–413, Aug. 2019.
- [16] A. Eklund, T. E. Nichols, and H. Knutsson, "Cluster failure: Why fMRI inferences for spatial extent have inflated false-positive rates," *Proc. Nat. Acad. Sci. U.S.A.*, vol. 113, no. 28, pp. 7900–7905, Jun. 2016.
- [17] W. Sun, B. J. Reich, T. T. Cai, M. Guindani, and A. Schwartzman, "False discovery control in large-scale spatial multiple testing," *J. Roy. Statist. Soc. Ser. B*, vol. 77, no. 1, pp. 59–83, Apr. 2014.
- [18] H. Shu, B. Nan, and R. Koeppe, "Multiple testing for neuroimaging via hidden markov random field," *Biometrics*, vol. 71, no. 3, pp. 741–750, May 2015.
- [19] B. Efron, R. Tibshirani, J. D. Storey, and V. Tusher, "Empirical Bayes analysis of a microarray experiment," *J. Amer. Statist. Assoc.*, vol. 96, no. 456, pp. 1151–1160, 2001.
- [20] B. Efron, "Local false discovery rates," Tech. Rep., 2005.
- [21] ———, "Microarrays, empirical Bayes and the two-groups model," *Statist. Sci.*, vol. 23, no. 1, pp. 1–22, Feb. 2008.
- [22] ———, *Large-Scale Inference: Empirical Bayes Methods for Estimation, Testing, and Prediction*, ser. Institute of Mathematical Statistics Monographs. Cambridge, UK: Cambridge University Press, 2010.
- [23] W. Tansey, O. Koyejo, R. A. Poldrack, and J. G. Scott, "False discovery rate smoothing," *J. Amer. Statist. Assoc.*, vol. 113, no. 523, pp. 1156–1171, Jun. 2018.
- [24] T. Halme, M. Gözl, and V. Koivunen, "Bayesian multiple hypothesis testing for distributed detection in sensor networks," in *Proc. 2019 IEEE Data Sci. Workshop*, IEEE, Jun. 2019.
- [25] M. Gözl, M. Muma, T. Halme, A. Zoubir, and V. Koivunen, "Spatial inference in sensor networks using multiple hypothesis testing and Bayesian clustering," in *Proc. 27th Eur. Signal Process. Conf.*, Sep. 2019, pp. 1–5.
- [26] J. G. Scott, R. C. Kelly, M. A. Smith, P. Zhou, and R. E. Kass, "False discovery rate regression: An application to neural synchrony detection in primary visual cortex," *J. Amer. Statist. Assoc.*, vol. 110, no. 510, pp. 459–471, Apr. 2015.
- [27] S. Chen and S. Kasiviswanathan, "Contextual online false discovery rate control," in *Proc. 23rd Int. Conf. Artif. Intell. Statist.*, ser. Proceedings of Machine Learning Research, vol. 108, PMLR, 26–28 Aug 2020, pp. 952–961.
- [28] O. Muralidharan, "An empirical Bayes mixture method for effect size and false discovery rate estimation," *Ann. Appl. Statist.*, vol. 4, no. 1, pp. 422–438, 2010.
- [29] R. Martin and S. T. Tokdar, "A nonparametric empirical Bayes framework for large-scale multiple testing," *Biostatistics*, vol. 13, no. 3, pp. 427–439, Nov. 2011.
- [30] A. Molisch, E. Biglieri, A. Goldsmith, L. Greenstein, N. Mandayam, and H. V. Poor, "Propagation issues for cognitive radio," in *Principles of Cognitive Radio*, Cambridge University Press, pp. 102–149.
- [31] S. Marano and A. H. Sayed, "Detection under one-bit messaging over adaptive networks," *IEEE Trans. Inf. Theory*, vol. 65, no. 10, pp. 6519–6538, Oct. 2019.
- [32] G. Rovatsos, V. V. Veeravalli, and G. V. Moustakides, "Quickest detection of a dynamic anomaly in a heterogeneous sensor network," in *2020 IEEE Int. Symp. Inf. Theory*, IEEE, Jun. 2020.
- [33] A. M. Zoubir and D. R. Iskander, *Bootstrap Techniques for Signal Processing*. Cambridge University Press, Jan. 2001.
- [34] M. Gözl, V. Koivunen, and A. Zoubir, "Nonparametric detection using empirical distributions and bootstrapping," in *Proc. 25th Eur. Signal Process. Conf.*, IEEE, Aug. 2017.
- [35] X. Chen, D. G. Robinson, and J. D. Storey, "The functional false discovery rate with applications to genomics," *Biostatistics*, vol. 22, no. 1, pp. 68–81, May 2019.
- [36] S. Pounds and S. Morris, "Estimating the occurrence of false positives and false negatives in microarray studies by approximating and partitioning the empirical distribution of p-values," *Bioinformatics*, vol. 19, pp. 1236–1242, Jan. 2003.
- [37] C. T. Le, W. Pan, and J. Lin, "A mixture model approach to detecting differentially expressed genes with microarray data," *Funct. Integra. Genomics*, vol. 3, no. 3, pp. 117–124, Jul. 2003.
- [38] S. Robin, A. Bar-Hen, J.-J. Daudin, and L. Pierre, "A semi-parametric approach for mixture models: Application to local false discovery rate estimation," *Comput. Stats. Data Anal.*, vol. 51, no. 12, pp. 5483–5493, Aug. 2007.
- [39] R. Martin, "On nonparametric estimation of a mixing density via the predictive recursion algorithm," 2018.
- [40] M. A. Newton, "On a nonparametric recursive estimator of the mixing distribution," *Sankhyā Ser. A*, vol. 64, no. 2, pp. 306–322, 2002.
- [41] A. P. Dempster, N. M. Laird, and D. B. Rubin, "Maximum likelihood from incomplete data via the em algorithm," *J. Roy. Statist. Soc. Ser. B*, vol. 39, no. 1, pp. 1–38, 1977.

- [42] K. Pearson, "Method of moments and method of maximum likelihood," *Biometrika*, vol. 28, no. 1/2, pp. 34–59, 1936.
- [43] D. R. Iskander and A. M. Zoubir, "Estimation of the parameters of the K-distribution using higher order and fractional moments [radar clutter]," *IEEE Trans. Aerosp. Electron. Syst.*, vol. 35, no. 4, pp. 1453–1457, 1999.
- [44] K. O. Bowman and L. R. Shenton, "Estimation: Method of moments," in *Encyclopedia of Statistical Sciences*. Hoboken, NJ, USA: Wiley, 2006.
- [45] D. Hsu and S. M. Kakade, "Learning mixtures of spherical gaussians: Moment methods and spectral decompositions," in *Proc. 4th Conf. Innov. Theor. Comput. Sci.*, Berkeley, California, USA: Association for Computing Machinery, 2013, pp. 11–20.
- [46] A. Anandkumar, D. Hsu, and S. M. Kakade, "A method of moments for mixture models and hidden markov models," in *Proc. 25th Annu. Conf. Learn. Theory*, vol. 23, Edinburgh, Scotland: JMLR Workshop and Conference Proceedings, 25–27 Jun 2012, pp. 33.1–33.34.
- [47] N. L. Johnson, S. Kotz, and N. Balakrishnan, *Continuous univariate distributions volume 2*. Hoboken, NJ, USA: Wiley, 1995, vol. 289.
- [48] R. Schaback, "A practical guide to radial basis functions," Tech. Rep., 2007.
- [49] G. E. Fasshauer, *Meshfree Approximation Methods with Matlab*. World Scientific, Apr. 2007.
- [50] J. Duchon, "Splines minimizing rotation-invariant semi-norms in sobolev spaces," in *Constructive Theory of Functions of Several Variables*, Springer Berlin Heidelberg, 1977, pp. 85–100.
- [51] W. Keller and A. Borkowski, "Thin plate spline interpolation," *J. Geod.*, vol. 93, no. 9, pp. 1251–1269, Feb. 2019.
- [52] D. Eberly, "Thin-plate splines," Geometric Tools, Tech. Rep., 2018.
- [53] X. Cai and G. Giannakis, "A two-dimensional channel simulation model for shadowing processes," *IEEE Trans. Veh. Technol.*, vol. 52, no. 6, pp. 1558–1567, Nov. 2003.